Supplementary Information: Informing NMR experiments with molecular dynamics simulations to characterize the dominant activated state of KcsA

Sergio Pérez-Conesa,[1, a)] Eric G. Keeler,[2, a)] Dongyu Zhang,[2, 3, a)] Lucie Delemotte,[1, b)] and Ann E. McDermott[2, b)]

[1)] *KTH Royal Institute of Technology, Science for Life Laboratory, Stockholm, Sweden*

[2)] *Department of Chemistry, Columbia University, New York, New York 10027, United States*

[3)] *Current Address:Plexxikon Inc., Berkeley, CA 94710, United States*

(Dated: 24 February 2021)

[a)] These three authors contributed equally

[b)] Correspondance to: lucied@kth.se, aem5@columbia.edu

I. SUPPLEMENTARY FIGURES

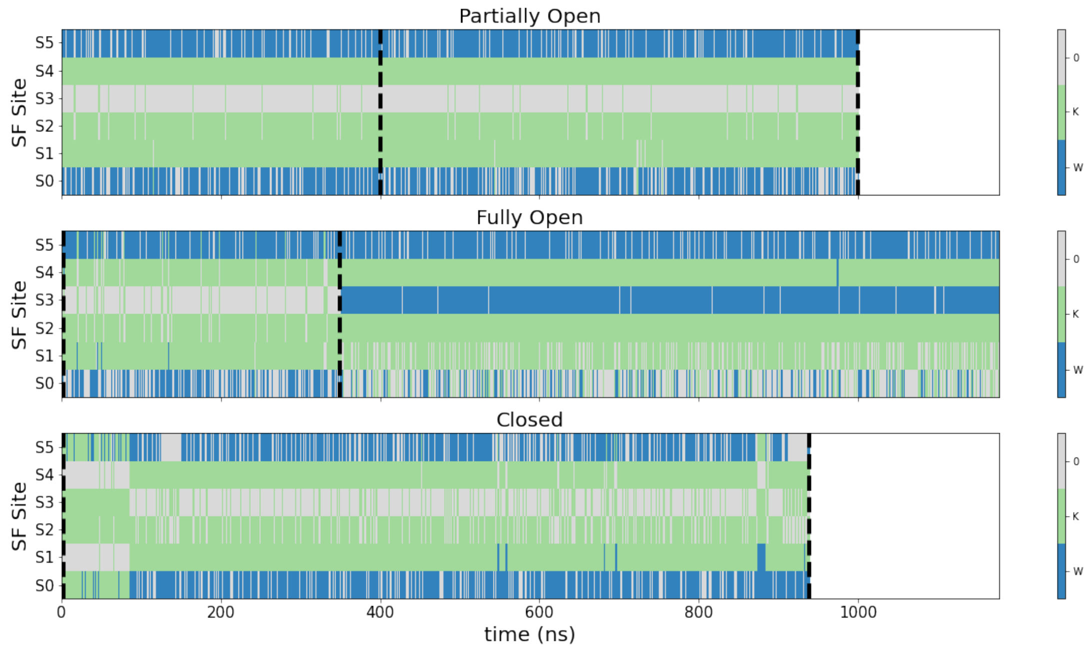

FIG. S1. Occupation of the canonical selectivity filter sites as a function of time in the MD simulations for the study states: Partially Open (top), Fully Open (middle) and Closed (bottom). For the Fully Open state the simulation data from the entry of a water molecule in the S3 site is discarded since this has been identified as a pre-inactivation sign.

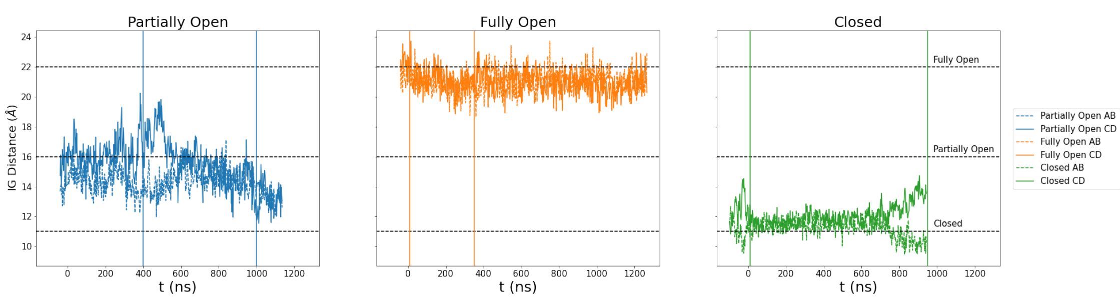

FIG. S2. Inner gate opening measured as the T112 C_α distance of opposing subunits (subunits AB solid line or subunits CD dashed line). Vertical lines delimit the part of the simulation analyzed. In the case of the partially open state the part with a more stable inner gate is used. For the Fully Open state this choice is based on selectivity filter occupation see Fig. S1. The data is smoothed with 50 point rolling median. Negative values of time are the equilibration period.

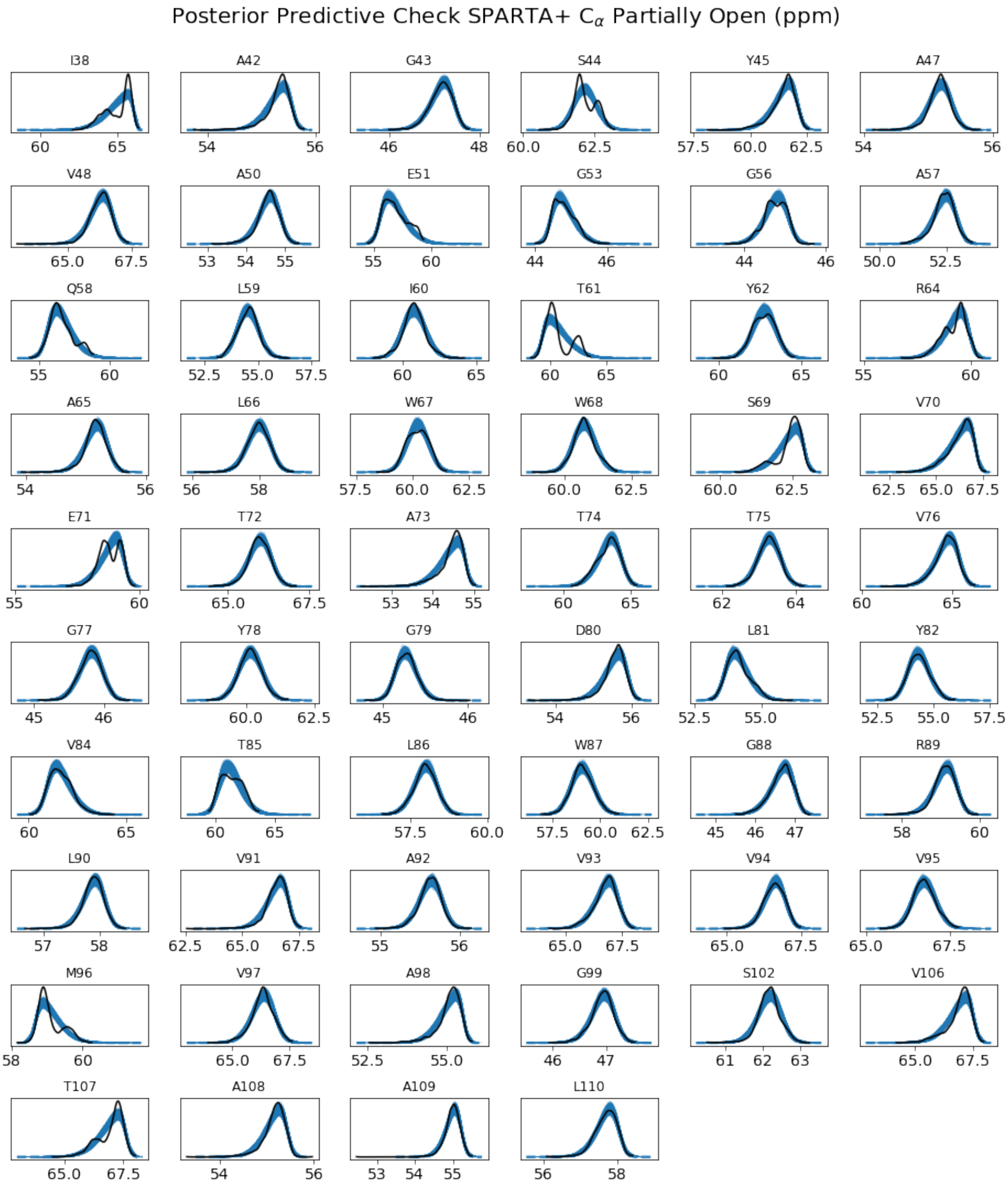

FIG. S3. Posterior predictive checks for C_α chemical shift data of the different residues calculated for the Partially Open state simulation with the CS prediction method SPARTA+. A posterior predictive check consists in sampling the posterior probability distributions (for our case the posteriors of μ, σ and α parameters since the likelihood is a skew-gaussian distribution) to produce an ensemble of distributions (blue lines) that are compared to the data used for the inference (dashed black line). Similar posterior predictive checks have been obtained for the rest of states, methods and nuclei and can be found in `https://github.com/delemottelab/Informing_NMR_experiments_w_MD`

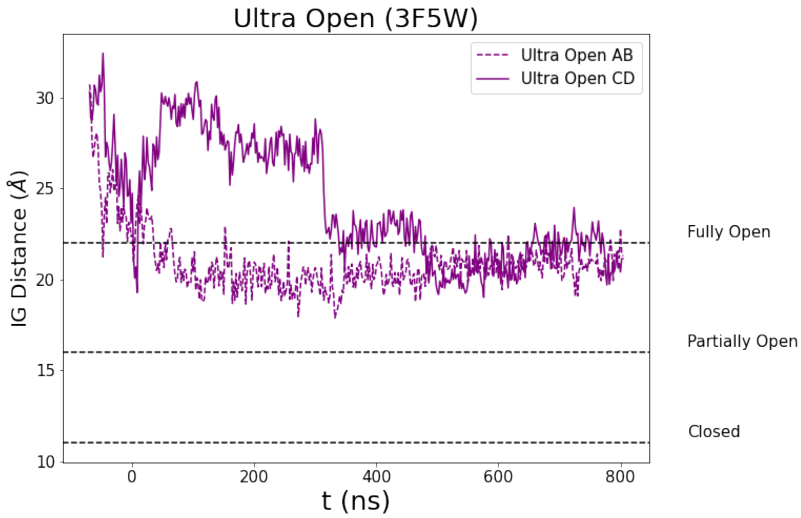

FIG. S4. Inner gate opening measured as the T112 C_α distance of opposing subunits (subunits AB solid line or subunits CD dashed line) for the "Ultra Open" structure (PDB ID 3F5W). The structure is unstable and the inner gate rapidly decays to openings compatible with the Fully Open state (PDB ID 5VK6). For this reason this simulation was not analyzed in this work.

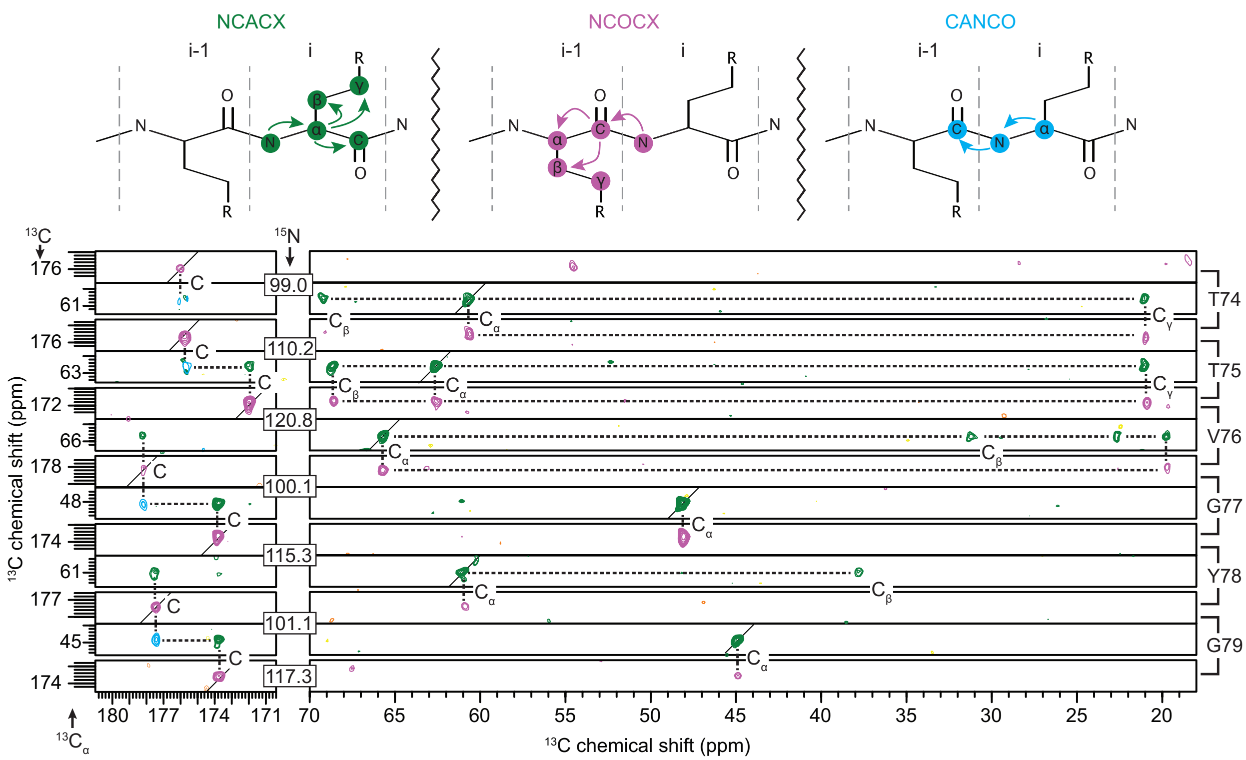

FIG. S5. Representative strip plot of the 3D experiments NCACX (green), NCOCX (magenta), CANCO (cyan) collected at 900 MHz that were used for the backbone walk of assignments of KcsA in the activated state (3:1 DOPE:DOPG, 50 mM KCl, pH 4.0). The polarization pathway of the experiments is shown (top). The backbone walk for residues T74 to G79 is shown.

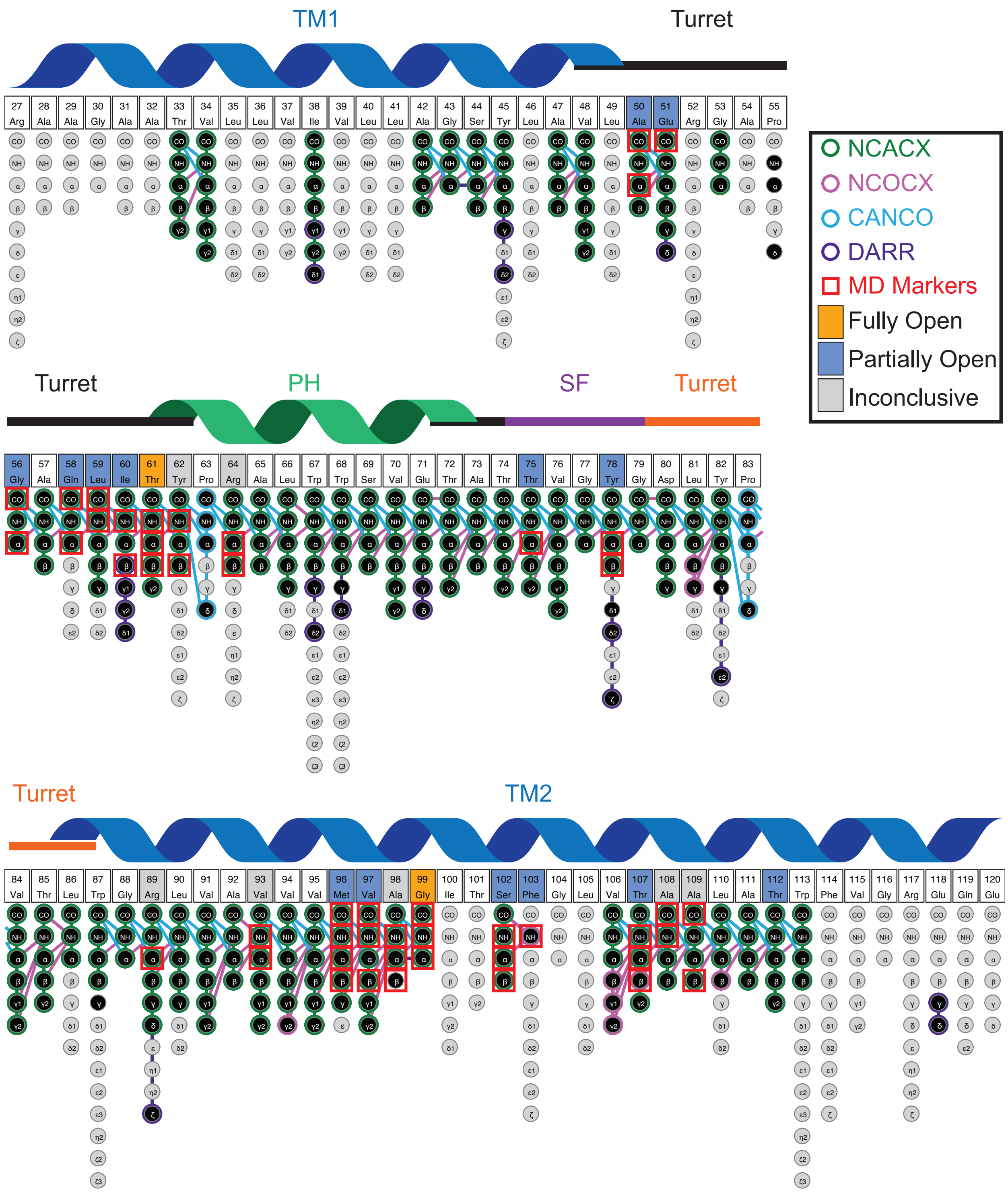

FIG. S6. Schematic indicating the assigned residues of KcsA in the activated state (3:1 DOPE:DOPG, 50 mM KCl, pH 4.0) with black filled in circles. The unassigned resonances are shown with gray filled circles. Open circles are used to indicate in which experiments the resonances are present. The 3D NCACX (green), NCOCX (magenta), and CANCO (cyan) and the 2D ^{13}C-^{13}C DARR (purple) are shown, other assigned peaks are present in other experimental spectra that are not indicated on this figure (ZF-TEDOR (Pro), NcoCX, NcaCX, NCO, NCA). The resonances identified by statistical inference on the MD simulation data to be state markers are indicated with a red square and the agreement with the various states (Fully Open - orange, Partially Open - blue, Inconclusive - gray) are shown on the residue name and number.

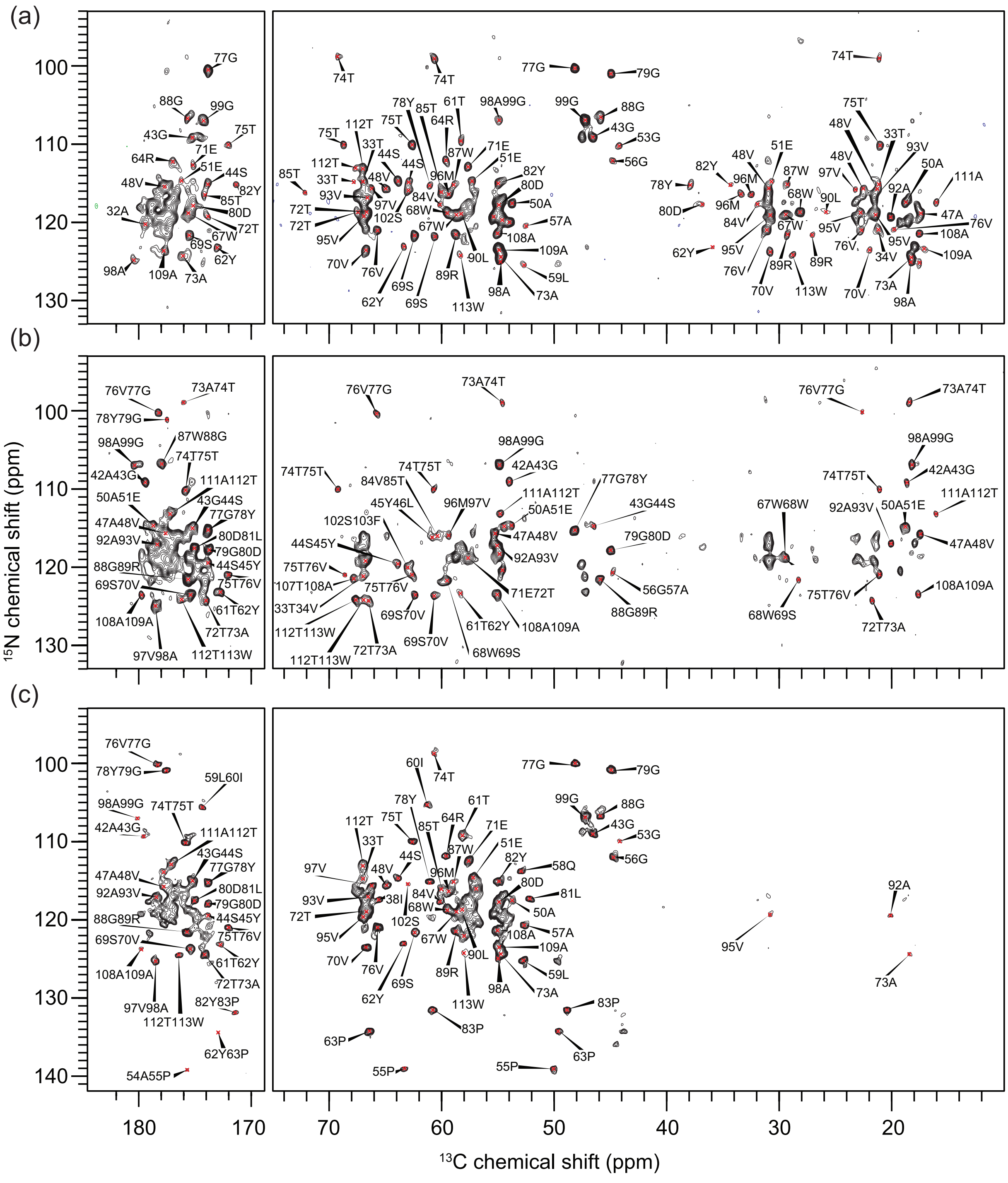

FIG. S7. 2D ^{13}C-^{15}N NcaCX (a), NcoCX (b), and ZF-TEDOR (c) spectra of KcsA in the activated state (3:1 DOPE/DOPG, 50 mM KCl, pH 4.0) spectra collected at 900 MHz (a and b) and 750 MHz (c). Assigned resonances are labeled as either N^{i}-C^{i} (NcaCX and ZF-TEDOR) or N^{i}-C^{i-1} (NcoCX and ZF-TEDOR).

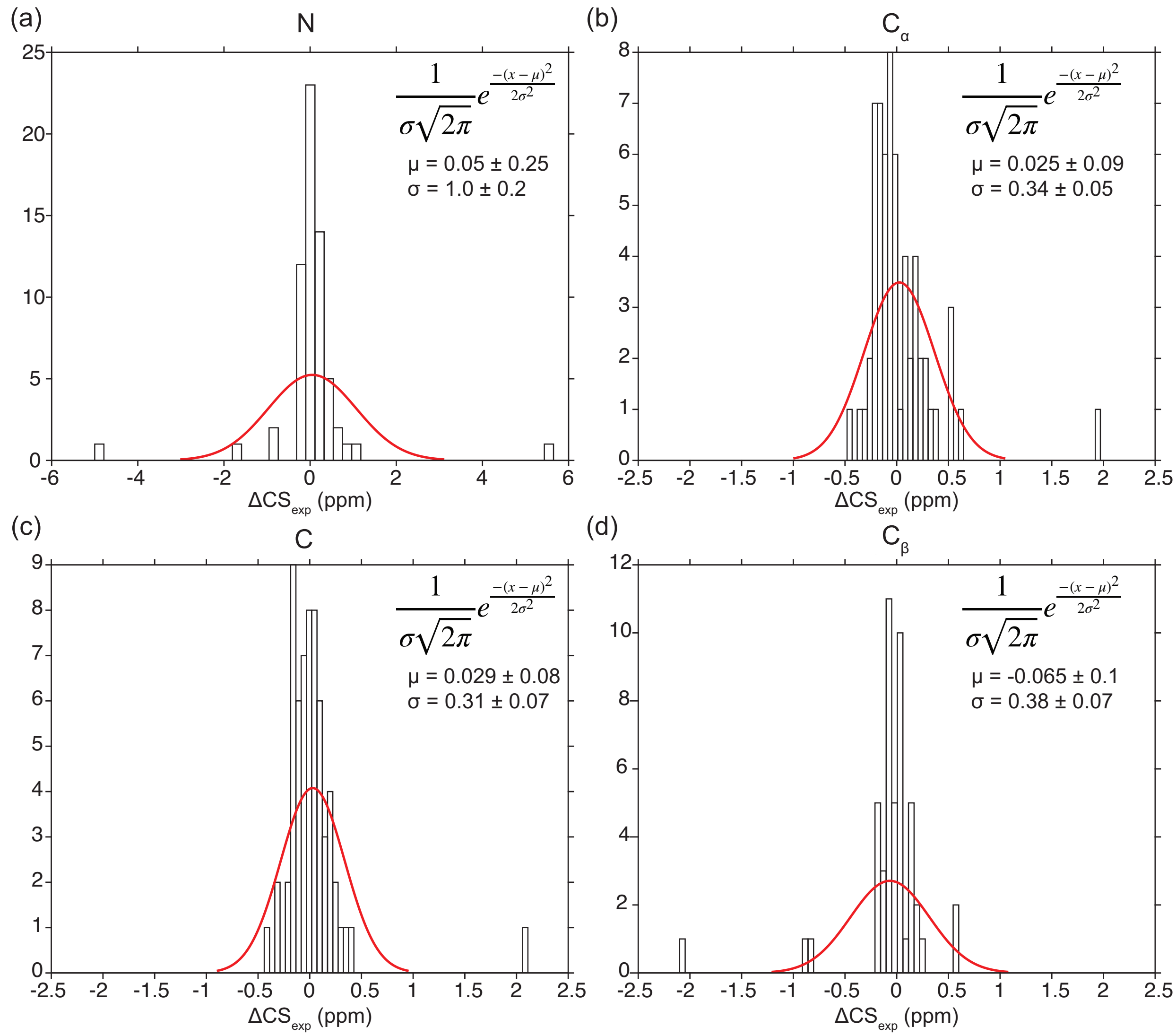

FIG. S8. Histograms of the experimental difference ($\Delta CS_{exp} = CS_{exp}^{pH=4,act} - CS_{exp}^{pH=7.5,deact}$) between the activated and deactivated state assigned chemical shifts for N (a), C (b), C_α (c), and C_β (d). A fitted normal distribution is shown on each histogram (red lines) with the distribution equation and parameters shown, inset, demonstrating the proper referencing of the datasets to one another.

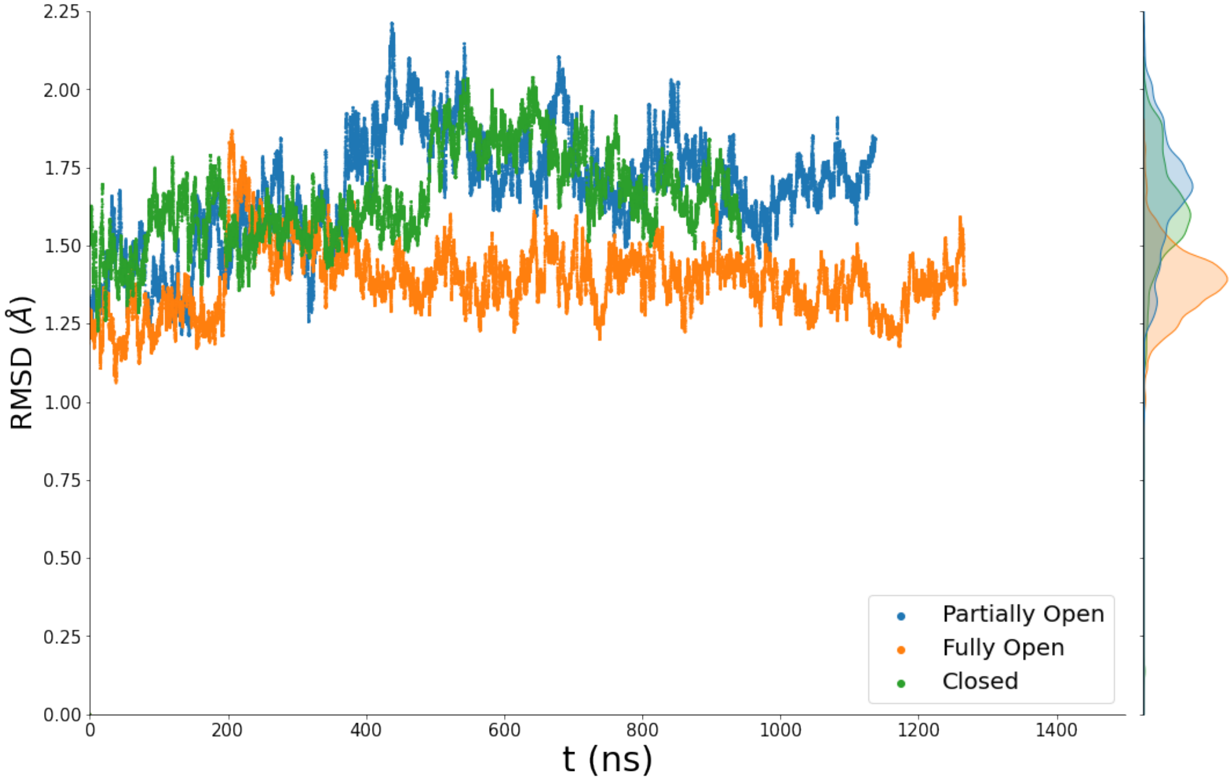

FIG. S9. Root mean square deviation (RMSD) of the C_α atom positions of the MD simulations as a function of time for the Partially Open, Fully Open and Closed states. Some of the noise is smoothed by a 10 step rolling median. Negative values of time are the equilibration period.

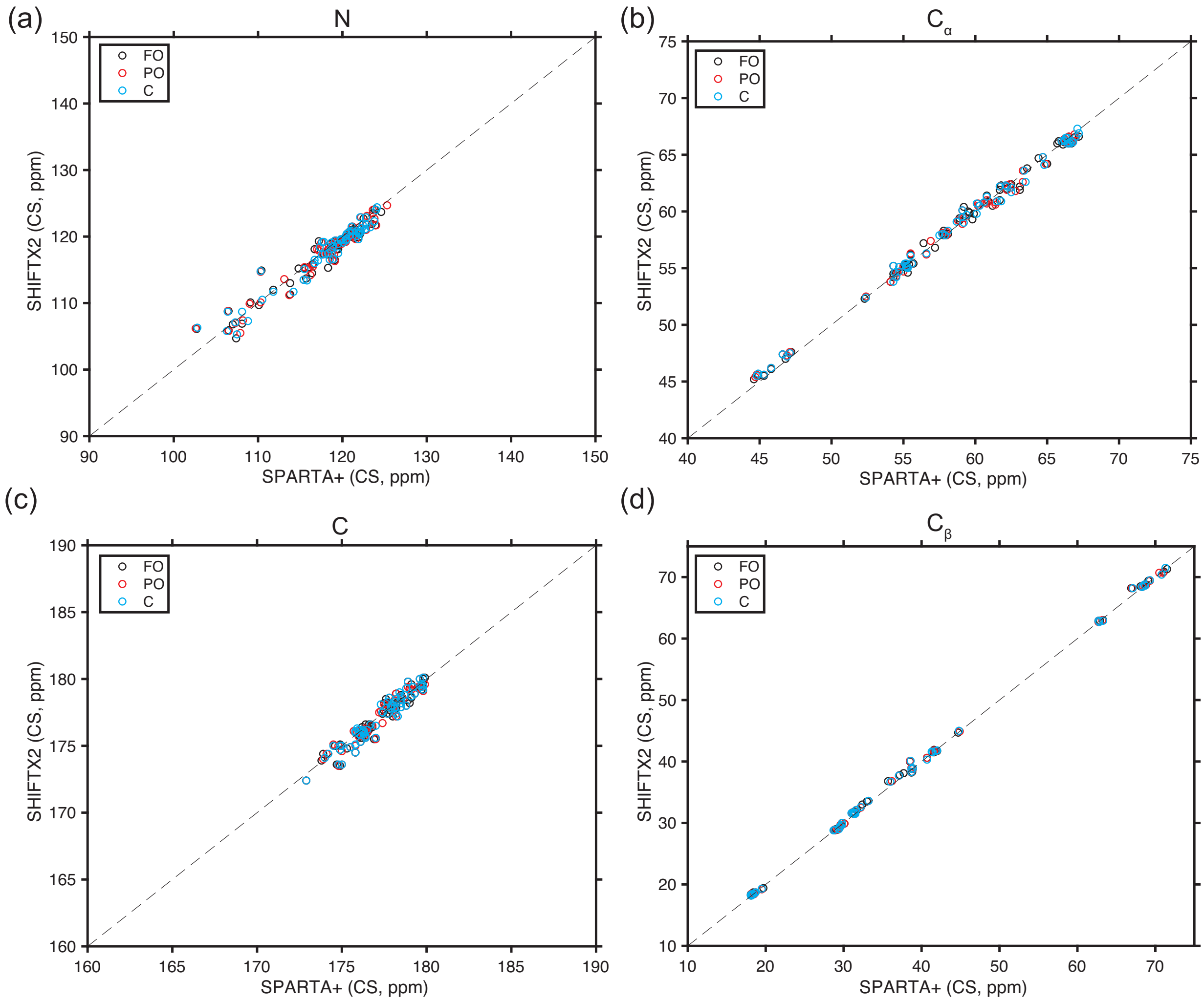

FIG. S10. Comparison of the predicted chemical shifts of the various states of KcsA (Fully Open - black, Partially Open - red, Closed - cyan) using SPARTA+ and SHIFTX2. The dashed line indicating perfect agreement is drawn for the eye.

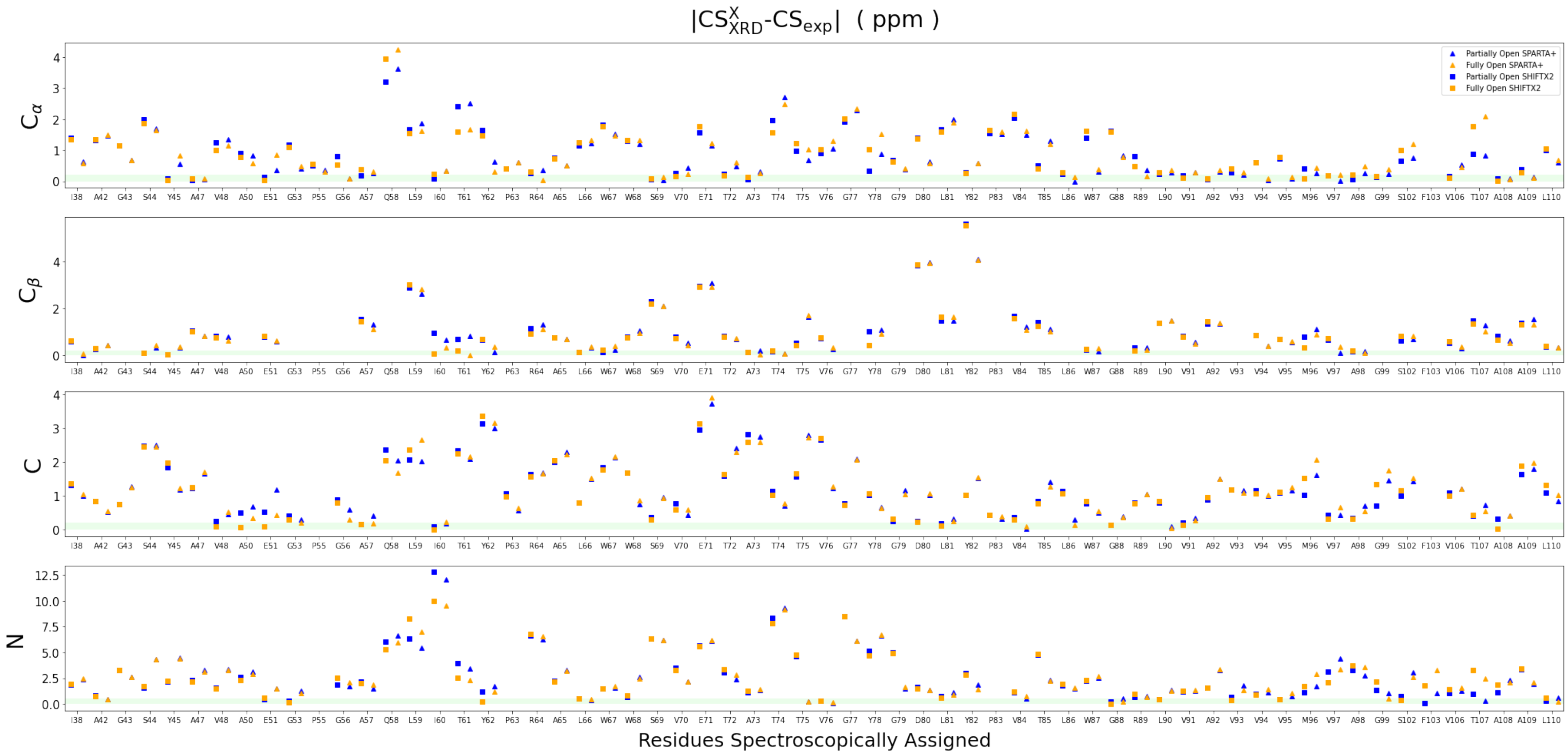

FIG. S11. Chemical shifts difference between experiment and the calculated CS for the XRD structures ($CS^{X}_{XRD} - CS_{exp}$), where X represents the FO (orange) or PO (blue) sate. All residues on the x-axis for the different nuclei and chemical shift prediction methods. The agreement between the calculation and the NMR experiments is higher the closer the value is to zero. Chemical shifts predicted by SPARTA+ and SHIFTX2 are drawn with triangles and squares respectively. The green shade depicts the typical experimental uncertainty.

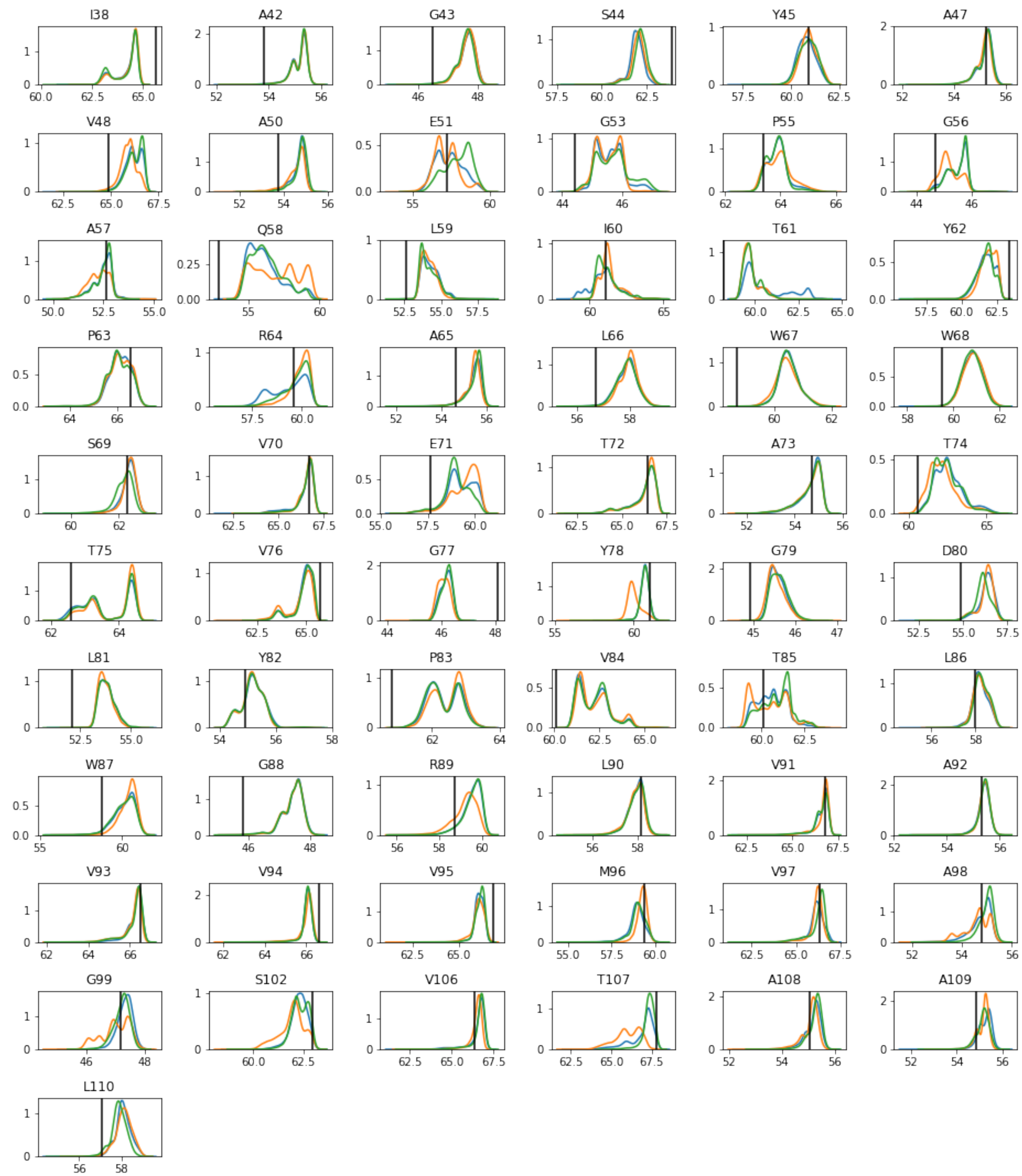

FIG. S12. Probability distributions of the raw simulated CS of the MD trajectory snapshots for the different residues assigned spectroscopically for the C_α nucleus and the CS prediction method SHIFTX2. Three different states are compared: Partially Open (blue), Fully Open (orange) and Closed (green). The distributions are calculated using kernel density estimation as implemented in the python library Seaborn.

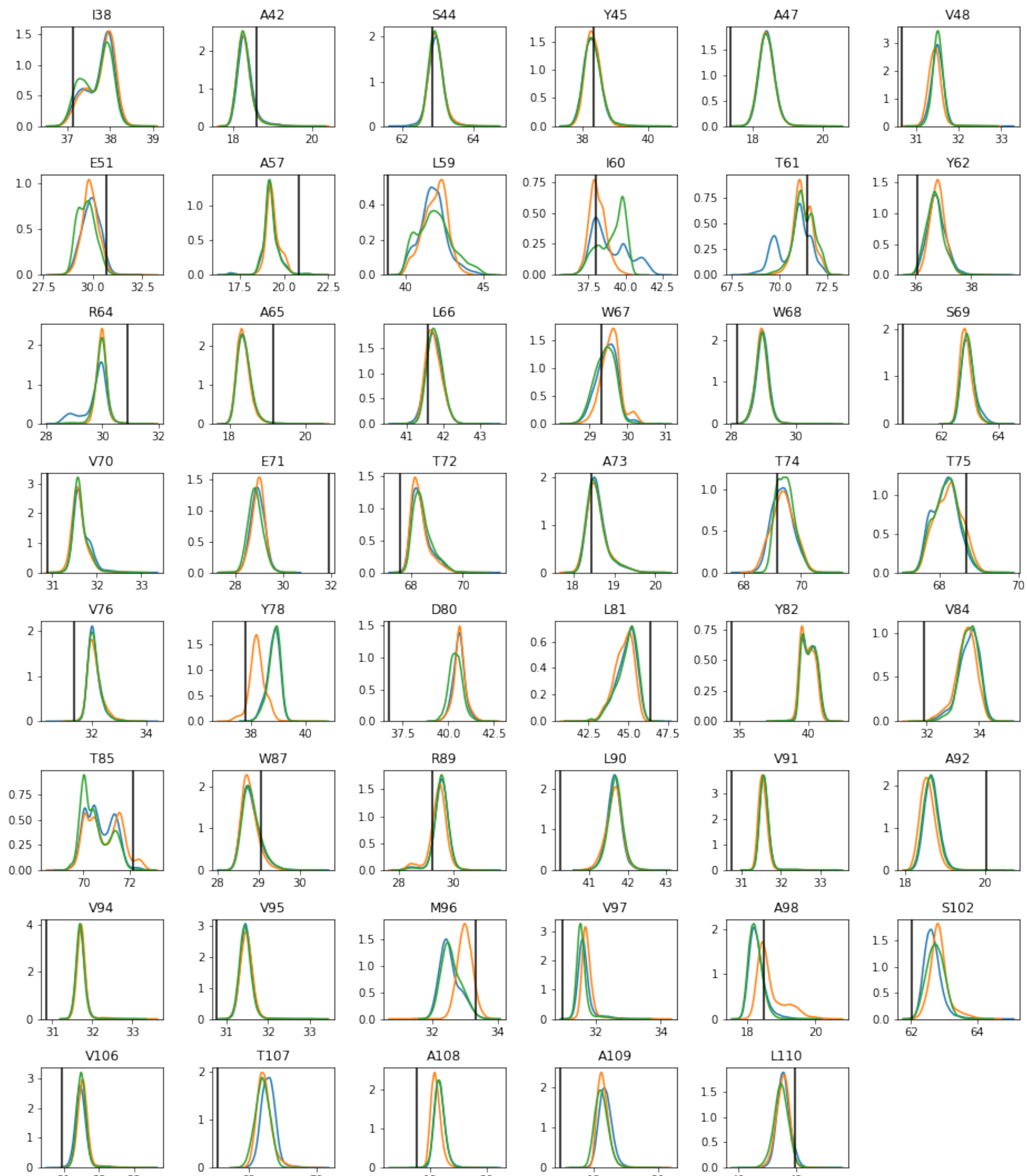

FIG. S13. Probability distributions of the raw simulated CS of the MD trajectory snapshots for the different residues assigned spectroscopically for the C_α nucleus and the CS prediction method SHIFTX2. Three different states are compared: Partially Open (blue), Fully Open (orange) and Closed (green). The distributions are calculated using kernel density estimation as implemented in the python library Seaborn.

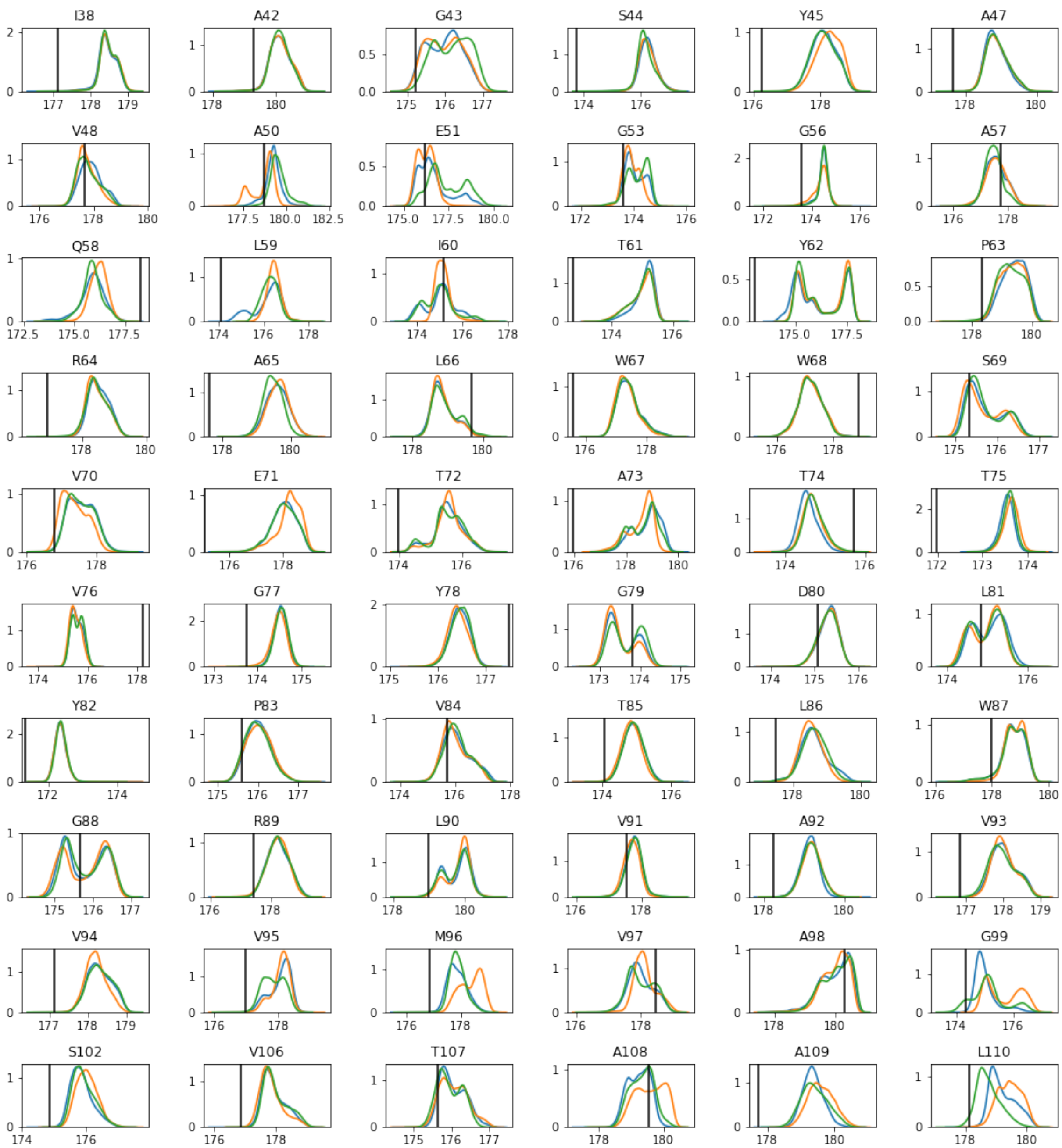

FIG. S14. Probability distributions of the raw simulated CS of the MD trajectory snapshots for the different residues assigned spectroscopically for the C nucleus and the CS prediction method SHIFTX2. Three different states are compared: Partially Open (blue), Fully Open (orange) and Closed (green). The distributions are calculated using kernel density estimation as implemented in the python library Seaborn.

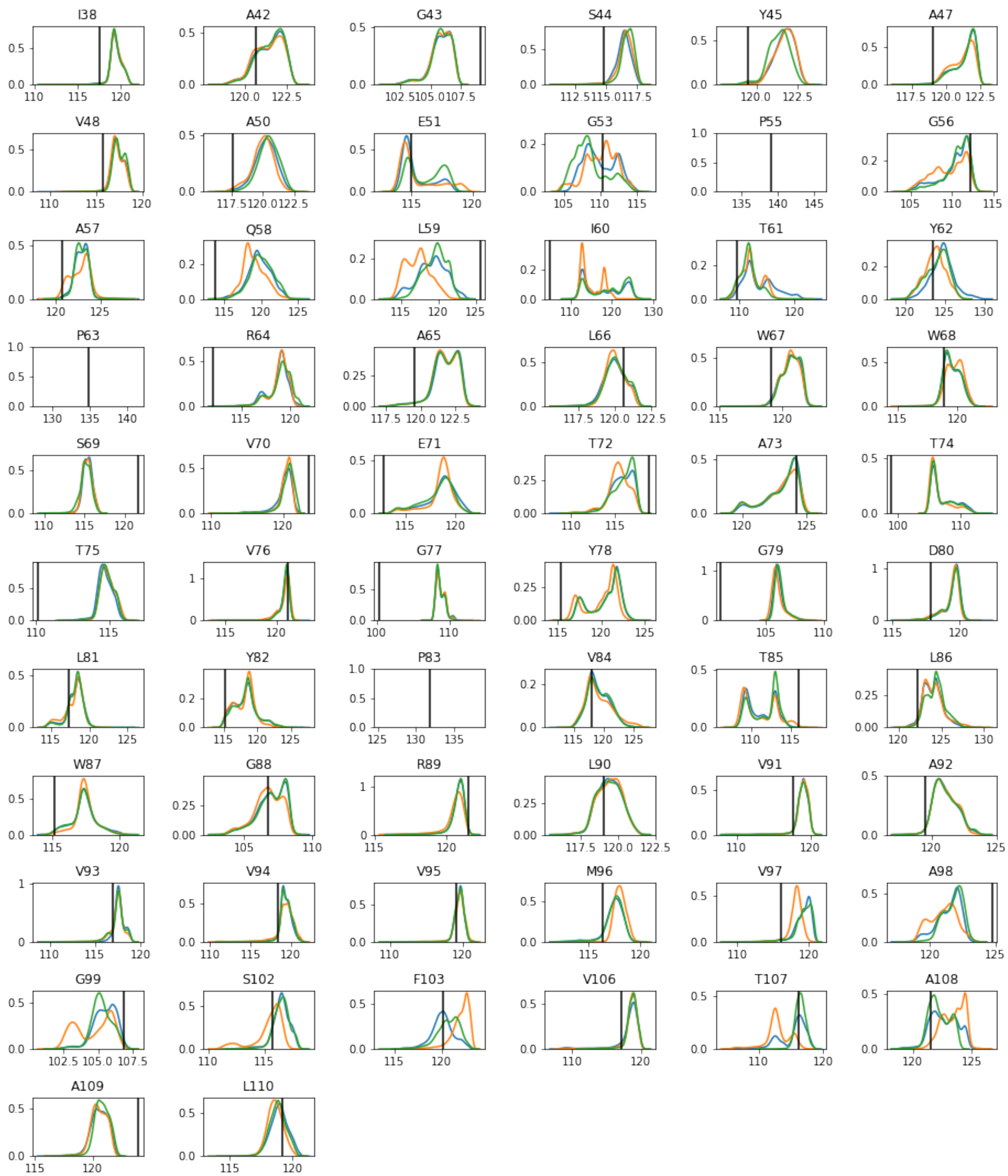

FIG. S15. Probability distributions of the raw simulated CS of the MD trajectory snapshots for the different residues assigned spectroscopically for the N nucleus and the CS prediction method SHIFTX2. Three different states are compared: Partially Open (blue), Fully Open (orange) and Closed (green). The distributions are calculated using kernel density estimation as implemented in the python library Seaborn.

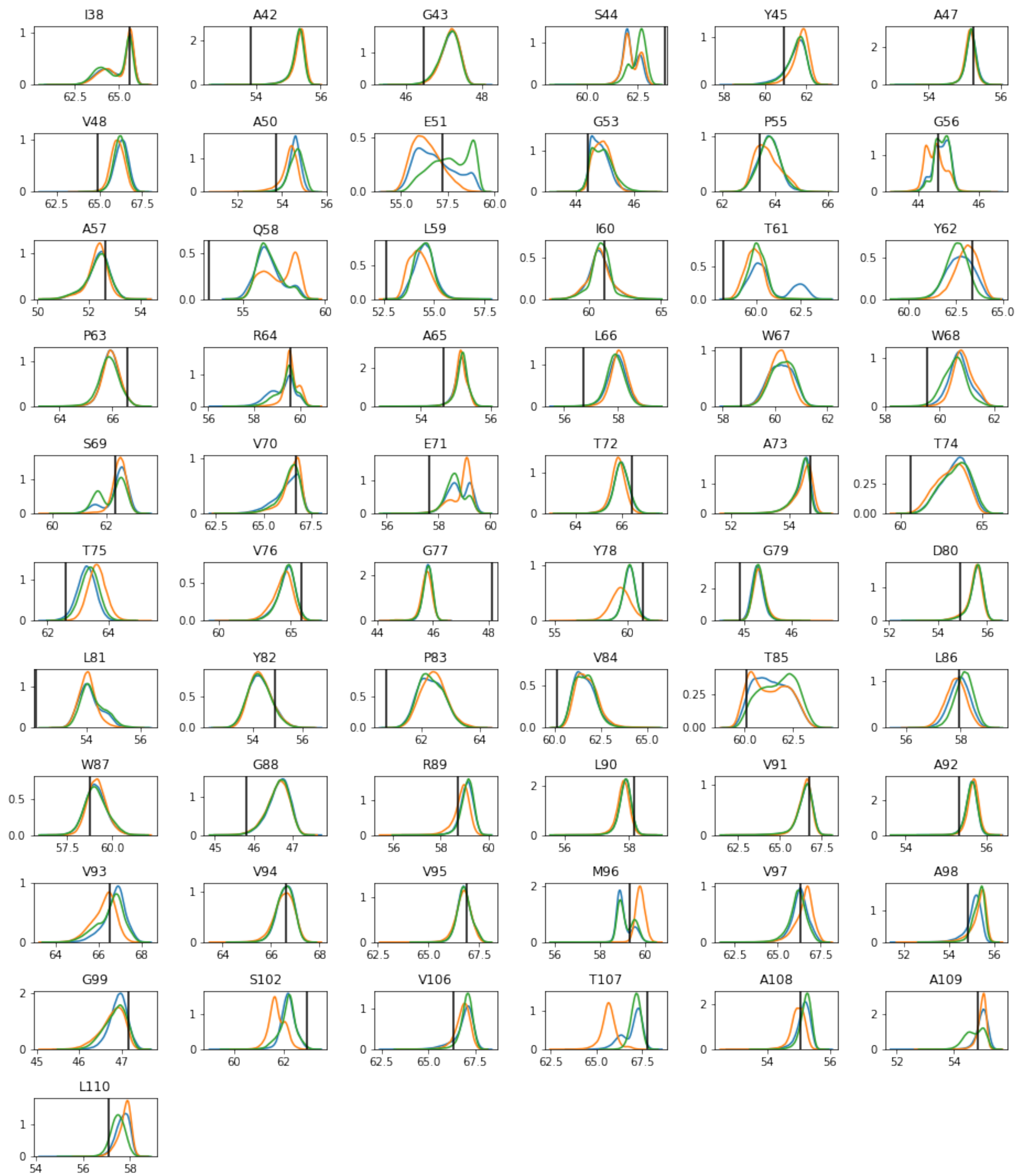

FIG. S16. Probability distributions of the raw simulated CS of the MD trajectory snapshots for the different residues assigned spectroscopically for the C_α nucleus and the CS prediction method SHIFTX2. Three different states are compared: Partially Open (blue), Fully Open (orange) and Closed (green). The distributions are calculated using kernel density estimation as implemented in the python library Seaborn.

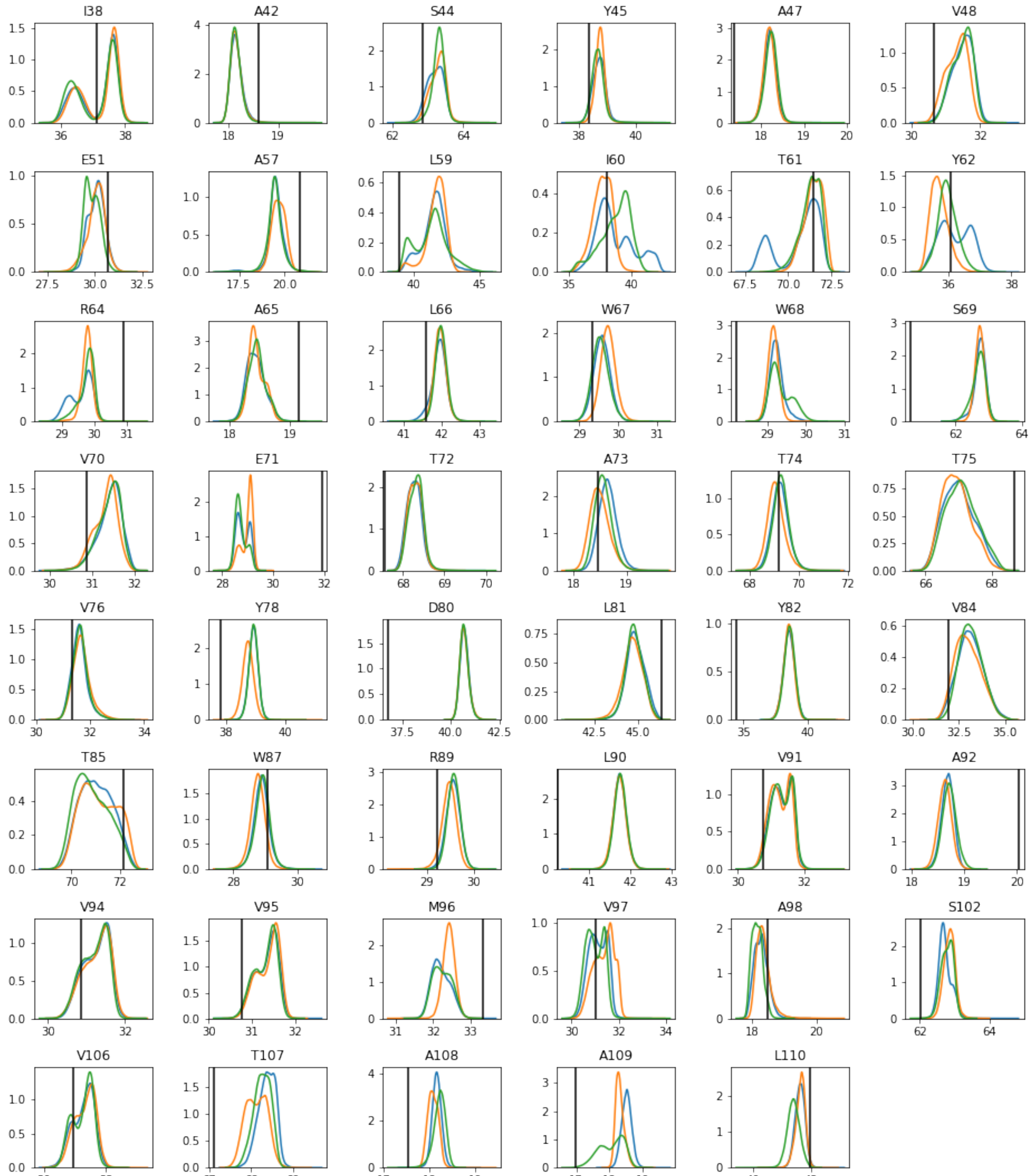

FIG. S17. Probability distributions of the raw simulated CS of the MD trajectory snapshots for the different residues assigned spectroscopically for the C_β nucleus and the CS prediction method SHIFTX2. Three different states are compared: Partially Open (blue), Fully Open (orange) and Closed (green). The distributions are calculated using kernel density estimation as implemented in the python library Seaborn.

FIG. S18. Probability distributions of the raw simulated CS of the MD trajectory snapshots for the different residues assigned spectroscopically for the C nucleus and the CS prediction method SHIFTX2. Three different states are compared: Partially Open (blue), Fully Open (orange) and Closed (green). The distributions are calculated using kernel density estimation as implemented in the python library Seaborn.

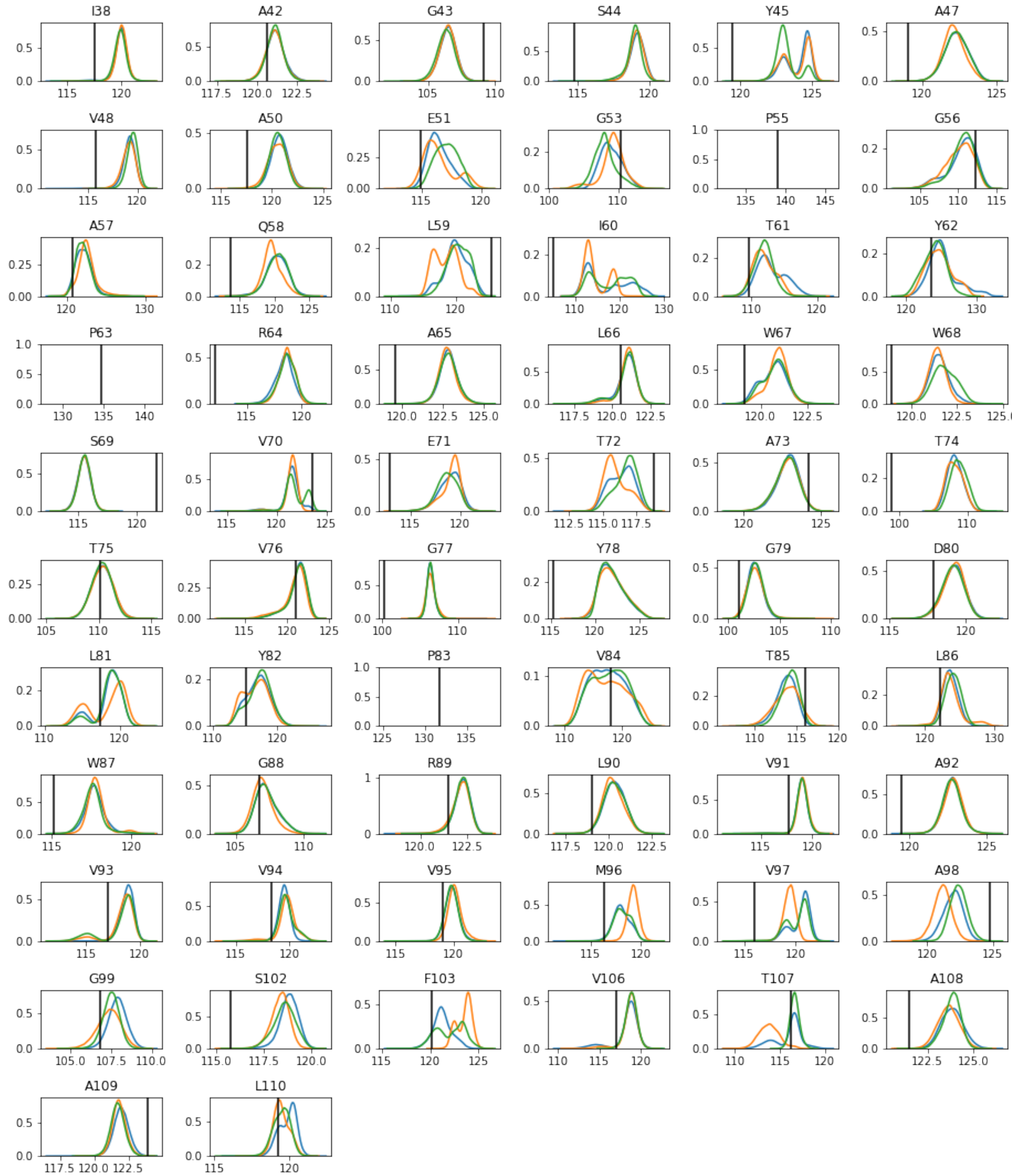

FIG. S19. Probability distributions of the raw simulated CS of the MD trajectory snapshots for the different residues assigned spectroscopically for the N nucleus and the CS prediction method SHIFTX2. Three different states are compared: Partially Open (blue), Fully Open (orange) and Closed (green). The distributions are calculated using kernel density estimation as implemented in the python library Seaborn.

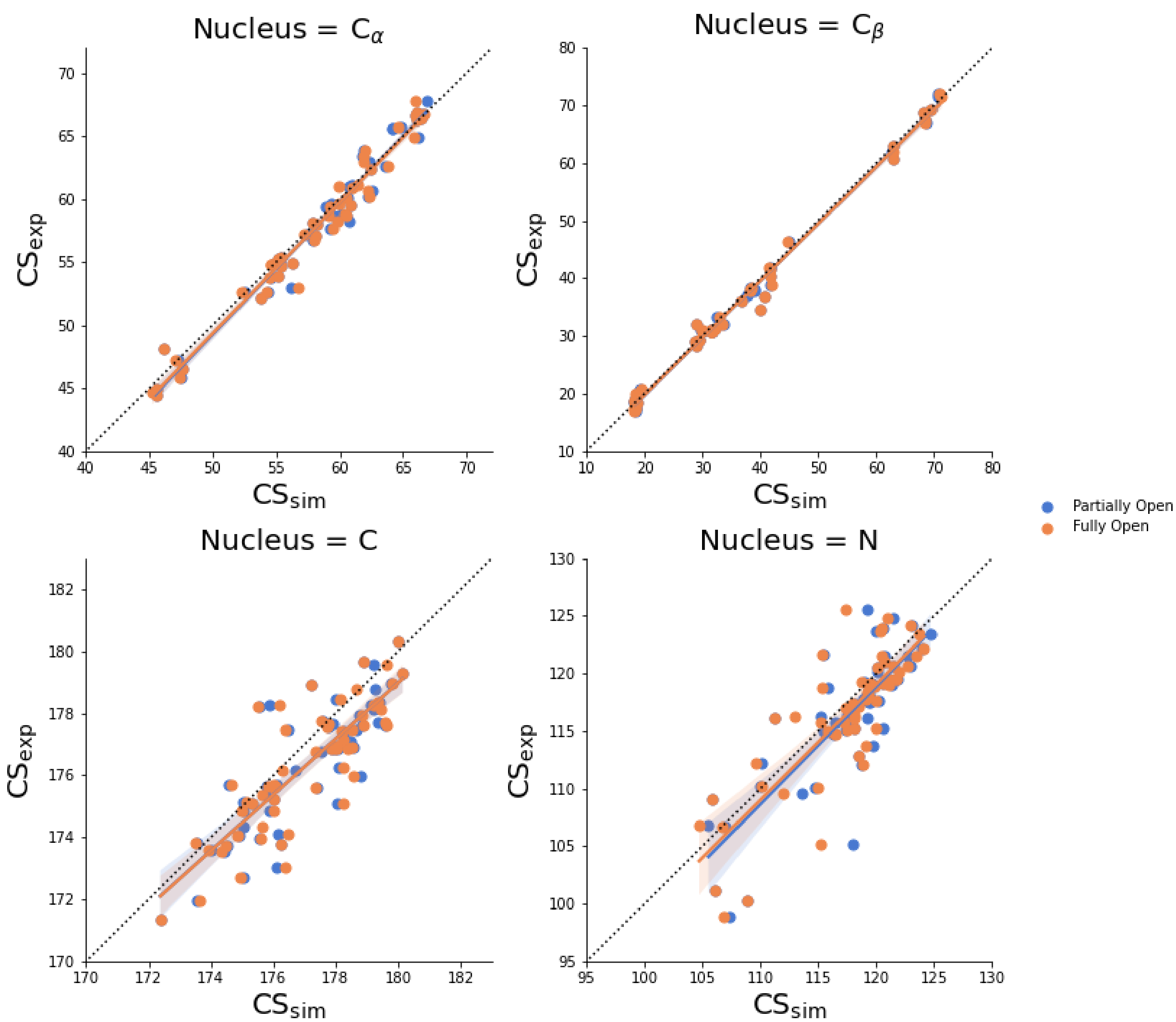

FIG. S20. Correlation diagram between experimental and simulated chemical shifts for the Partially Open (blue) and Fully Open (orange) states for the nuclei studied and for the chemical shift prediction method SHIFTX2.

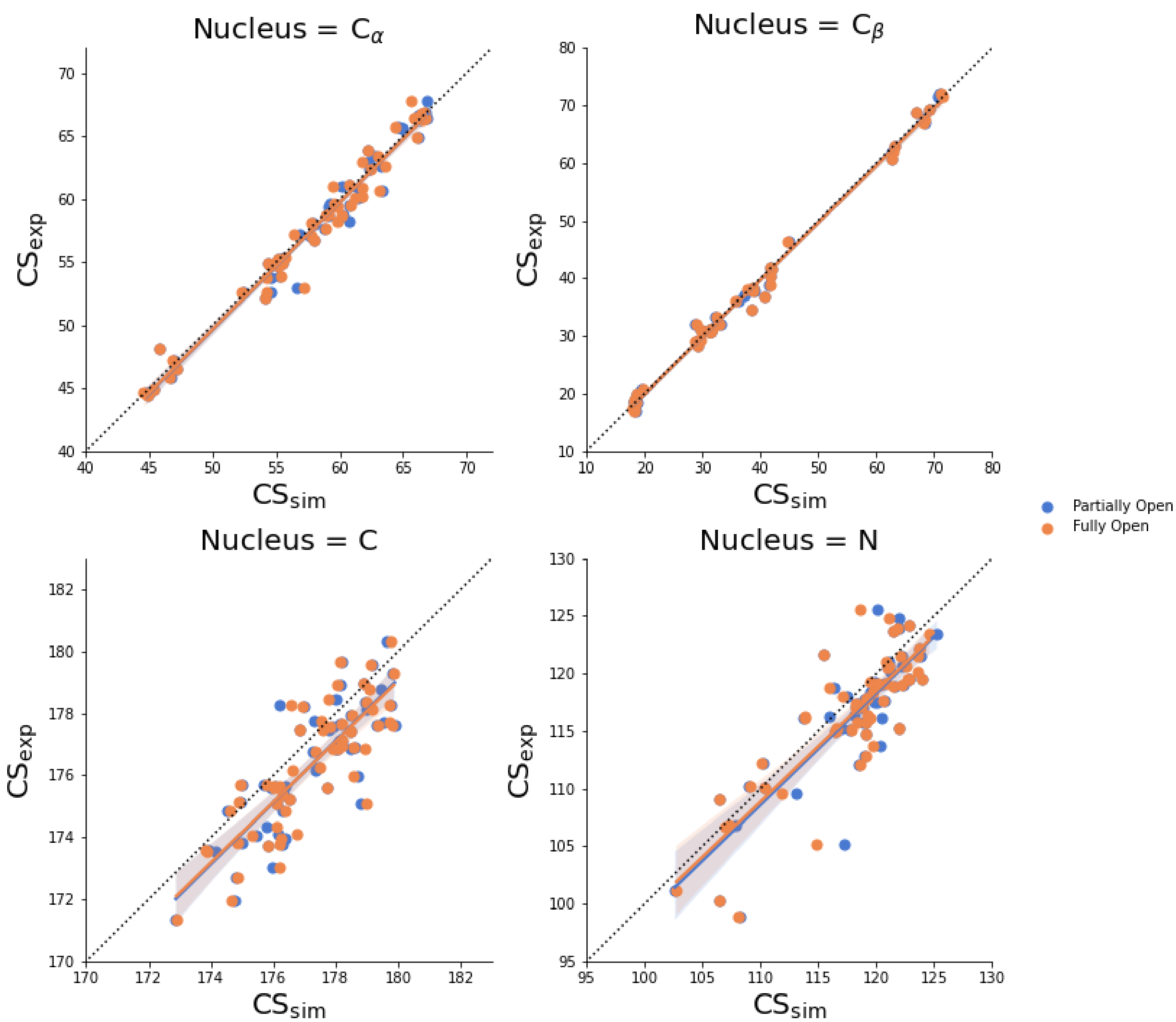

FIG. S21. Correlation diagram between experimental and simulated chemical shifts for the Partially Open (blue) and Fully Open (orange) states for the nuclei studied and for the chemical shift prediction method SPARTA+.

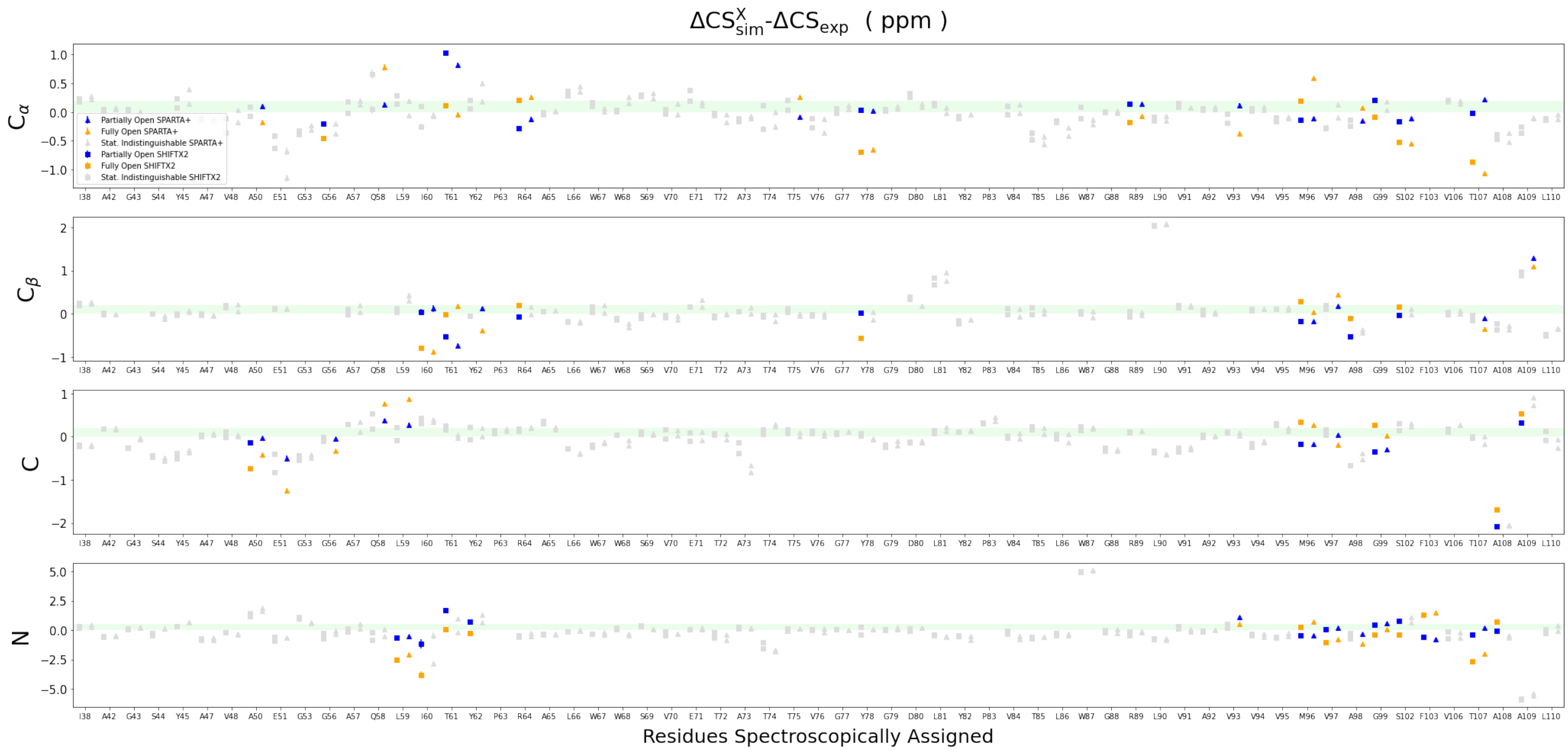

FIG. S22. Centers of 94% credible intervals of the difference in relative chemical shifts between experiment and simulation ($\Delta CS^{X}_{sim} - \Delta CS_{exp}$). The limits of the credible interval are shown as error bars. Both experiment and simulation use as reference the closed state chemical shifts: $\Delta CS^{X}_{sim} = CS^{X}_{sim}$ - CS^{C}_{sim} and $\Delta CS_{exp} = CS^{pH=4}_{exp}$ - $CS^{pH=7.5}_{exp}$, where X represents the FO or PO sate. All residues on the x-axis for the different nuclei and chemical shift prediction methods. The agreement between MD simulations and the NMR experiments is higher the closer the value is to zero. Chemical shifts predicted by SPARTA+ and SHIFTX2 are drawn with triangles and squares respectively. The PO state (blue) has in general a better agreement with experiment than FO state (orange). The green shade depicts the typical experimental uncertainty. If two methods produce statistically identical CS or the signal is missing in the spectrum, the symbols are represented in gray.

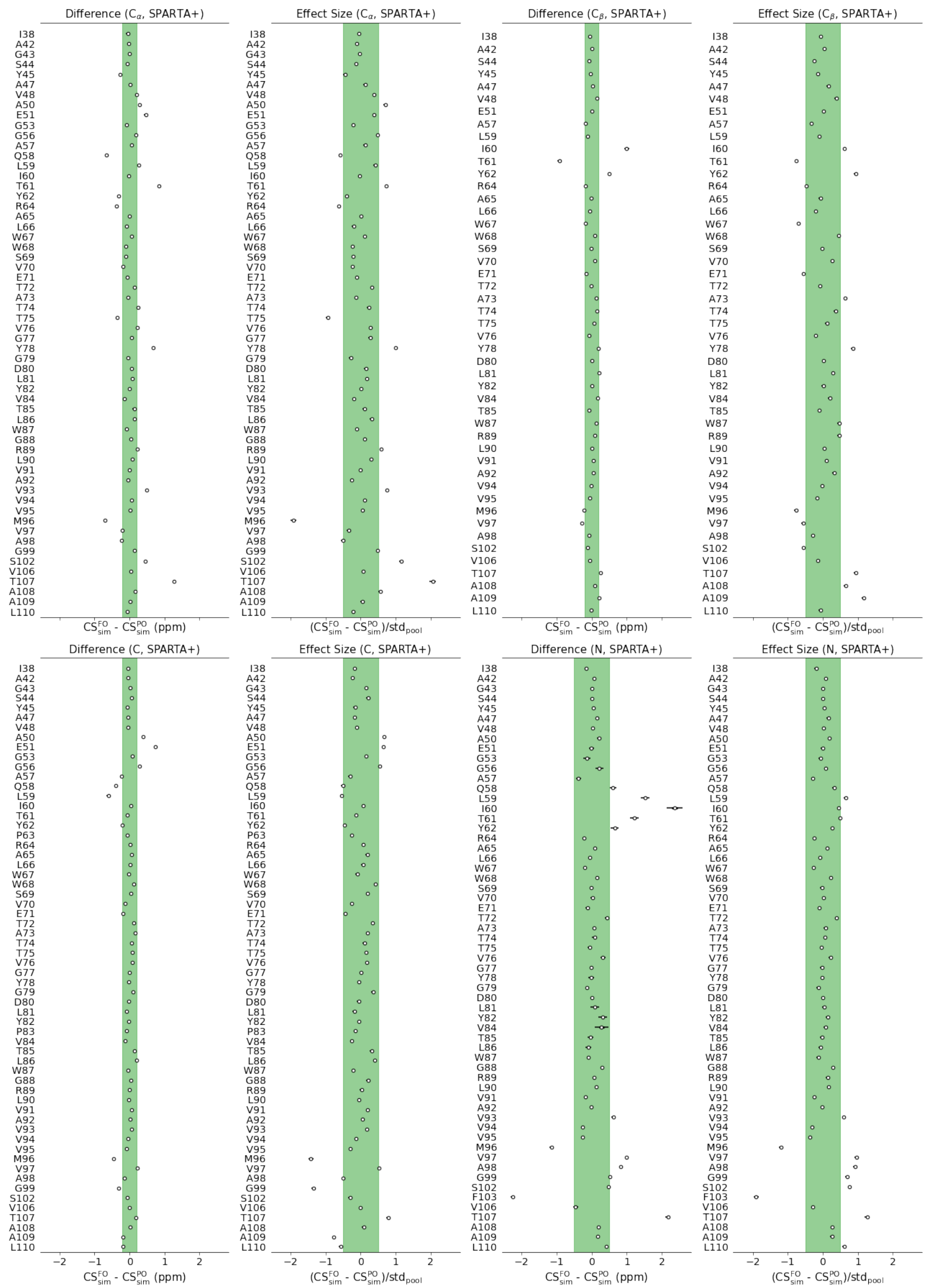

FIG. S23. Statistical filtering of simulated signals to discover discriminating residues using the CS prediction method SPARTA+. Horizontal bars represent the 94% credible interval of the variable distributions and circles represent its center.

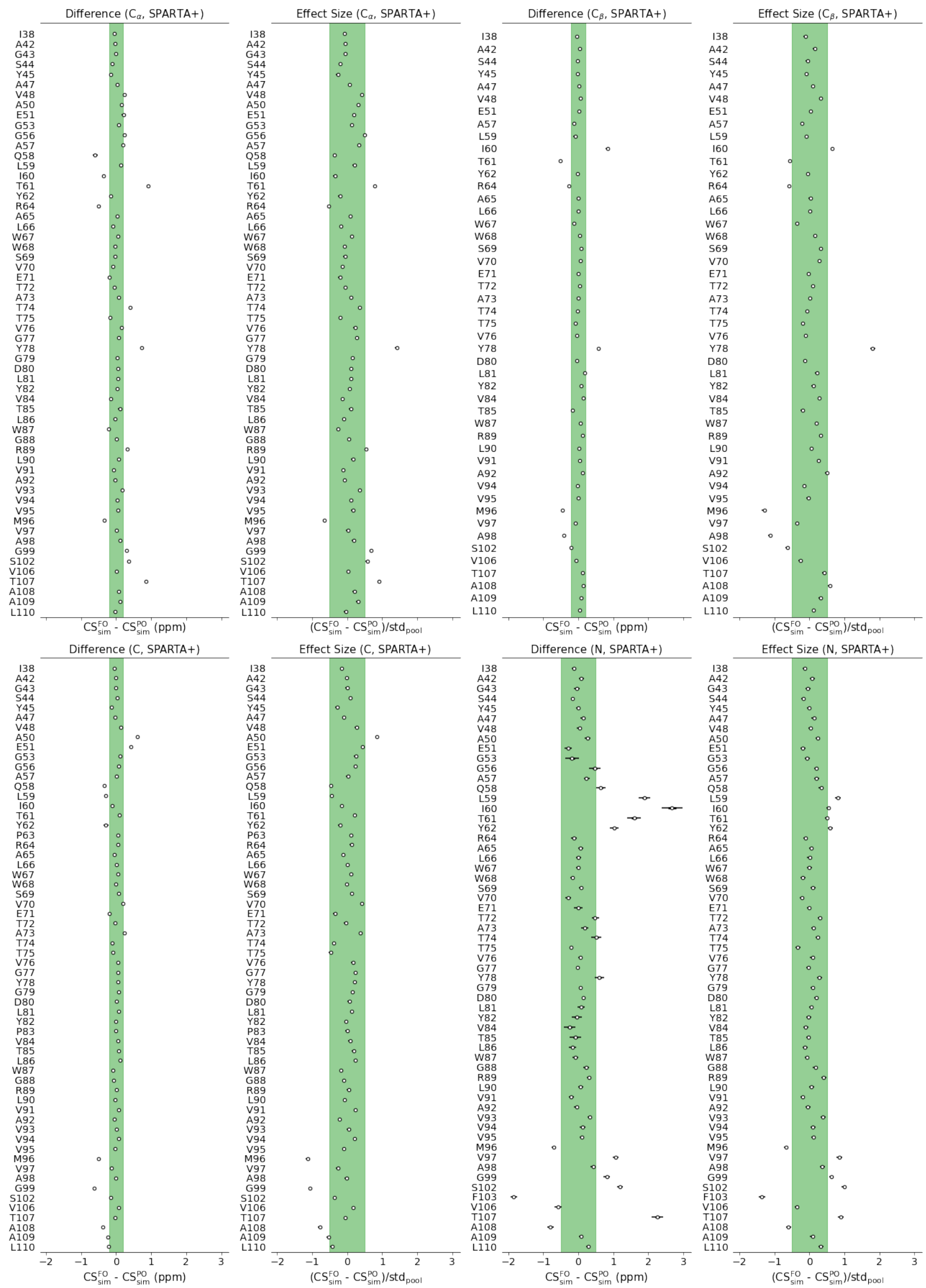

FIG. S24. Statistical filtering of simulated signals to discover discriminating residues using the CS prediction method SHIFTX2. Horizontal bars represent the 94% credible interval of the variable distributions and circles represent its center.

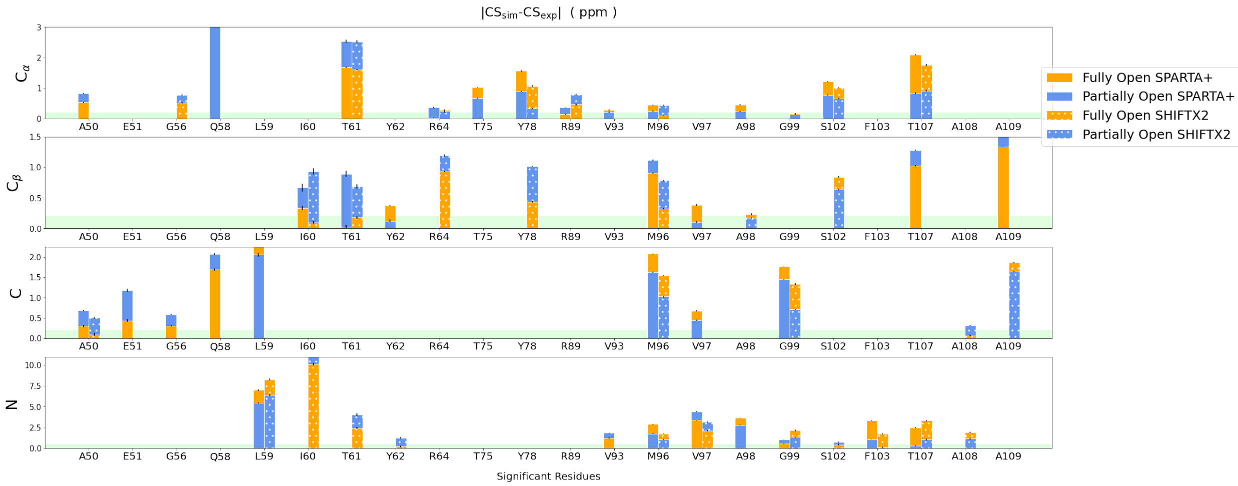

FIG. S25. Centers 94% credible intervals of the difference in chemical shifts between experiment and simulation in absolute value ($|CS^{X}_{sim} - CS_{exp}|$). The limits of the credible interval are shown as error bars. The residues found to be discriminating residues using our statistical criteria are represented on the x-axis for the different nuclei and chemical shift prediction methods. The agreement to experiment is higher the closer the value is to zero. The green shade depicts the typical experimental uncertainty. The absence of a reference state increases the noise in the data.

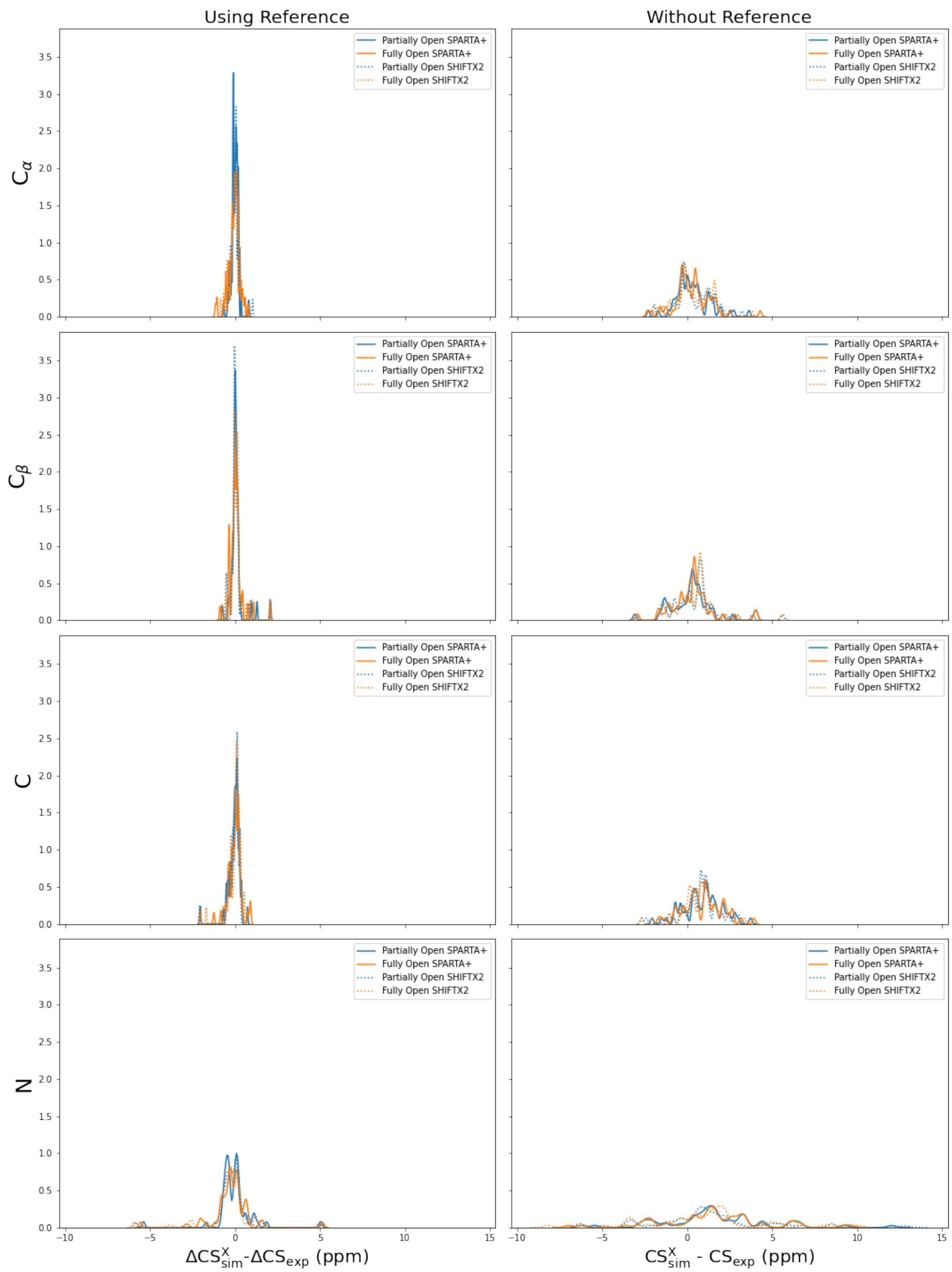

FIG. S26. Distributions of the CS simulation-experiment difference for the different nuclei (rows), for the two CS prediction methods (SPARTA+ solid line and SHIFTX2 dotted line) and for the two conductive states (Partially Open, blue and Fully Open, orange). These differences with experiment can be done using the CS of the closed state as a reference ($\Delta CS^X_{sim} - \Delta CS_{exp}$, left column) or without a reference ($CS^X_{sim} - CS_{exp}$ right column). The distributions without using the closed reference state are sharper and therefore using a reference state cancels random and systematic errors. The distributions are calculated using kernel density estimation as implemented in the python library Seaborn.

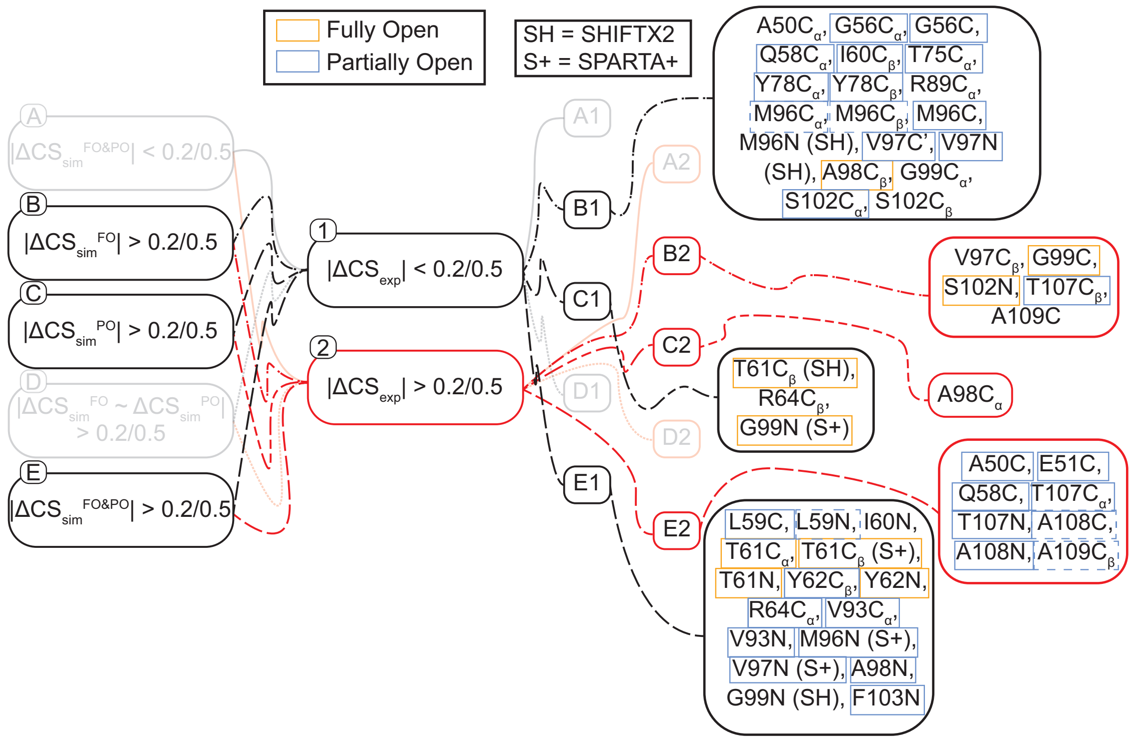

FIG. S27. Flow chart demonstrating the combinations of the ΔCS^{X}_{sim} and ΔCS_{exp} that yield various classifications of the state markers identified in this study. A threshold of tolerance of 0.2 ppm for ^{13}C and 0.5 ppm for ^{15}N was used to determine if the CS change was significant. The resonances that are identified by Bayesian inference from the MD simulation data as distinguishing between FO and PO are shown, on the right, within the classification that they were determined to belong. Two different classifications for each state marker are possible due to the two chemical shift prediction tools. These are marked with what chemical shift prediction tool was used for each resonance and classification type (SH = SHIFTX2 and S+ = SPARTA+). The state that determined to be likely based on the calculation of $\Delta\Delta CS^{X}$ is shown as an orange (FO) and blue (PO) box. Dashed boxes are used to indicate when one CS prediction tool was inconclusive and the other determined a state. Resonances that were determined to be inconclusive are shown without a thin box around them. FO = fully open, PO = partially open, C = closed, $\Delta CS^{X}_{sim} = CS^{X}_{sim}$ - CS^{Closed}_{sim}, and $\Delta CS_{exp} = CS^{pH=4,\ act}_{exp}$ - $CS^{pH=7.5,\ deact}_{exp}$.

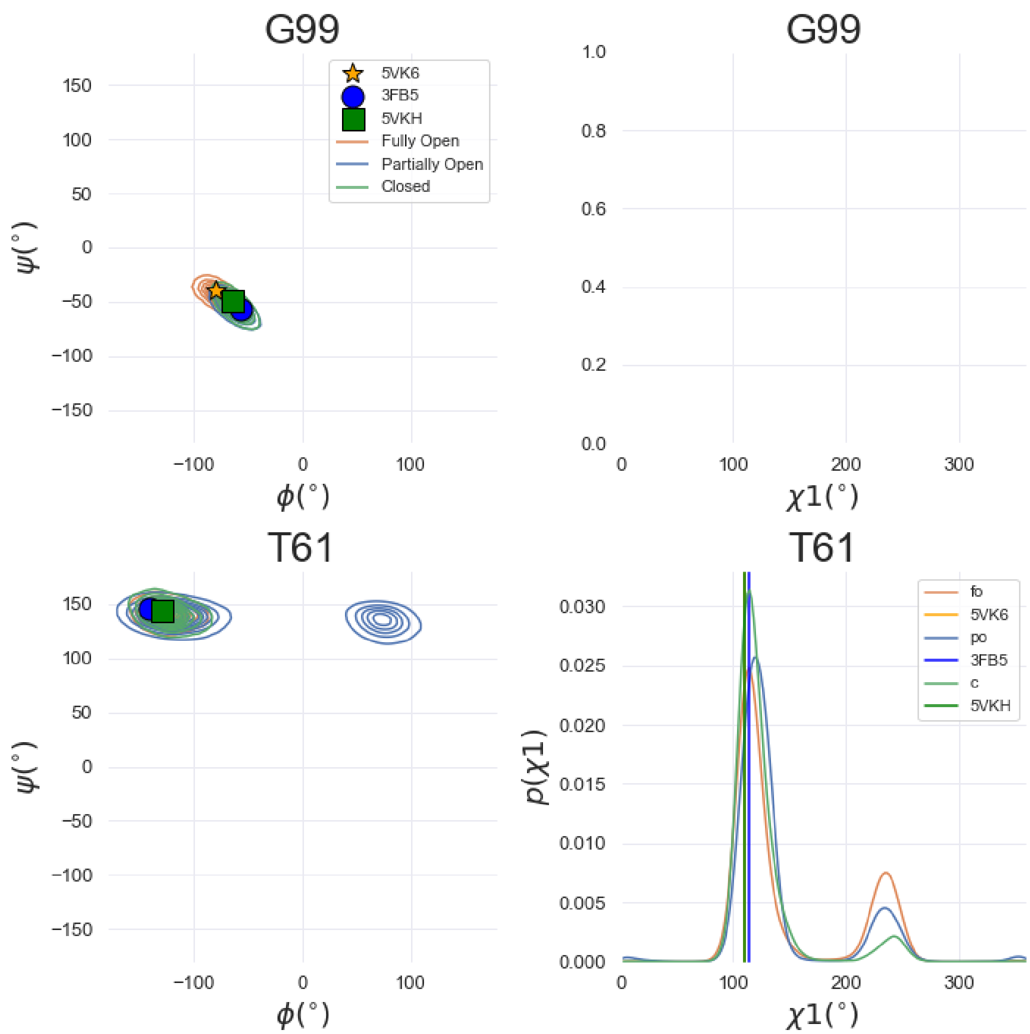

FIG. S28. Ramachandran and Janin diagrams (left and right columns, respectively) of the discriminating amino acids (rows) that are consistent with the Fully Open state as opposed to the Partially Open state consistent with most markers. The distributions are obtained from the dihedral angles obtained from the simulations of the Fully Open, Partially Open and Closed states. Additionally the values of the XRD structures are included as points or vertical lines.. Kernel density estimation is used to calculate the distributions as implemented in the Seaborn python library.

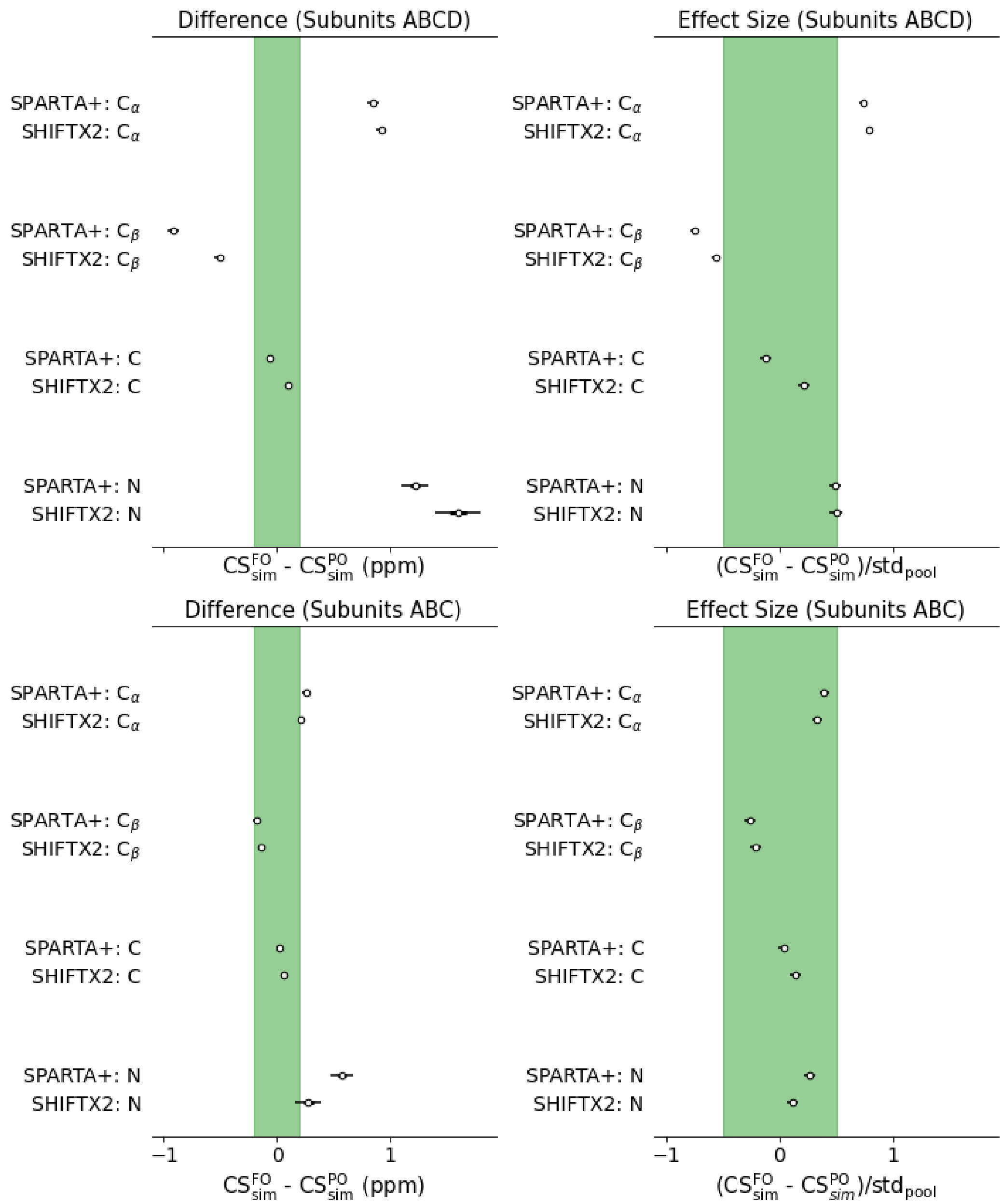

FIG. S29. Statistical filtering variables: difference in means and effect size for residue T61. The top graphs show the data using the four subunits of KcsA and the bottom graphs only subunits ABC. This figure shows that the reason why T61 is a discriminating residue is because one of the subunits has fluctuated away from the average. Horizontal bars represent the 94% credible interval of the variable distributions and circles represent its center.

II. SUPPLEMENTARY TABLES

TABLE S1: Experimental parameters for the 3D experiments at 900 MHz. Pulse sequences similar to those used for these experiments are available at `comdnmr.nysbc.org`

Experiment		3D NCACX	3D NCOCX	3D CANCO
MAS frequency		16 kHz	16 kHz	16.666 kHz
First transfer		H-N CP	H-N CP	H-C CP
	$\omega_{1,\mathrm{H}}/2\pi$ (kHz)	62	62	69
	$\omega_{1,\mathrm{N/C}}/2\pi$ (kHz)	N:50	N:50	C:59
	Pulse shape	^{1}H tangential	^{1}H tangential	Linear ramp
	Contact time (ms)	0.8	0.8	0.8
Second transfer		N-C CP	N-C CP	C-N CP
	$\omega_{1,\mathrm{H}}/2\pi$ (kHz)	94	91	91
	$\omega_{1,\mathrm{N/C}}/2\pi$ (kHz)	C: 28 N: 42	C: 41 N: 25	C: 29 N: 42
	Shape: nucleus and range	^{13}C tangential	^{13}C tangential	^{13}C tangential
	Contact time (ms)	5	5.2	5.5
Third transfer		C-C mixing	C-C mixing	N-C CP
	$\omega_{1,\mathrm{H}}/2\pi$ (kHz)	17	17	98
	$\omega_{1,\mathrm{N/C}}/2\pi$ (kHz)			C: 43 N: 25
	Shape: nucleus and range			^{13}C tangential
	Contact time (ms)	50	50	4.5
	$\omega_{1,\mathrm{H}}/2\pi$			91
Scans		16	32	64
Points	^{13}C (direct)	2048	2048	2048
	^{13}C	248	110	50
	^{15}N	60	80	48
Acquisition time	^{13}C (direct) (ms)	12.3	12.3	12.3
	^{13}C (ms)	6.6	6.6	7.2
	^{15}N (ms)	7	7.2	6

Sweep width	^{13}C (direct) (ppm)	368	368	368
	^{13}C (ppm)	74	37	37
	^{15}N (ppm)	50	46	46
Carrier Frequency	^{13}C (direct) (ppm)	100.8	100.8	175.8
	^{13}C (ppm)	60.8	175.8	60.8
	^{15}N (ppm)	118.1	118.1	118.1
Total time		5 d 12 h	8 d	7 d 14 h

TABLE S2: Experimental parameters for the 3D experiments at 750 MHz. Pulse sequences similar to those used for these experiments are available at `comdnmr.nysbc.org`

Experiment		3D NCACX	3D NCOCX	3D CANCO
MAS frequency		16 kHz	16 kHz	33.333 kHz
First transfer		H-N CP	H-N CP	H-C CP
	$\omega_{1,H}/2\pi$ (kHz)	72	72	80
	$\omega_{1,N/C}/2\pi$ (kHz)	N:58	N:58	C:56
	Pulse shape	^{1}H tangential	^{1}H tangential	^{1}H tangential
	Contact time (ms)	1	1	1
Second transfer		N-C CP	N-C CP	C-N CP
	$\omega_{1,H}/2\pi$ (kHz)	95	95	95
	$\omega_{1,N/C}/2\pi$ (kHz)	C: 24 N: 40	C: 8 N: 24	C: 17 N: 48
	Shape: nucleus and range	^{13}C tangential	^{13}C tangential	^{13}C tangential
	Contact time (ms)	3.75	5.0	3.75
Third transfer		C-C mixing	C-C mixing	N-C CP
	$\omega_{1,H}/2\pi$ (kHz)	16	16	95
	$\omega_{1,N/C}/2\pi$ (kHz)			C: 17 N: 49
	Shape: nucleus and range			^{13}C tangential

	Contact time (ms)	50	50	5.0
	$\omega_{1,\mathrm{H}}/2\pi$			95
Scans		96	144	64
Points	^{13}C (direct)	2000	2000	2100
	^{13}C	90	60	130
	^{15}N	32	32	36
Acquisition time	^{13}C (direct) (ms)	12.8	12.8	13.44
	^{13}C (ms)	5.625	5.625	7.02
	^{15}N (ms)	6	6	7.8
Sweep width	^{13}C (direct) (ppm)	414	414	414
	^{13}C (ppm)	42.4	28.3	44.2
	^{15}N (ppm)	35	35	33.7
Carrier Frequency	^{13}C (direct) (ppm)	109.9	109.9	109.9
	^{13}C (ppm)	58	176.5	58
	^{15}N (ppm)	111.2	111.2	111.2
Total time		5 d 1 h	5 d 21 h	5 d 7 h

TABLE S3: Experimental resonance assignments of KcsA in the activated state (50 mM KCl, pH 4.0, 3:1 DOPE/DOPG)

Residue	**N**	**C**	**C$_\alpha$**	**C$_\beta$**	**C$_{\gamma 2}$**	**C$_{\gamma 2}$**	**C$_\delta$**	**C$_\varepsilon$**	**C$_\zeta$**
T33	114.86	175.04	66.88	67.65	21.15				
V34	120.9	177.17	66.88	30.86	23.11	21.28			
L35									
L36									
V37									
I38	117.52	177.12	65.62	37.14	28.74	16.72	13.36		
V39									
L40									
L41									

Residue	N	C	C_α	C_β	$C_{\gamma 2}$	$C_{\gamma 2}$	C_δ	C_ε	C_ζ
A42	120.63	179.3	53.82	18.6					
G43	109.11	175.24	46.47						
S44	114.79	173.76	63.88	62.85					
Y45	119.48	176.26	60.9	38.36	127.63		131.78		
L46									
A47	119.02	177.63	55.23	17.36					
V48	115.78	177.66	64.91	30.67	22.54	21.11			
L49									
A50	117.62	178.76	53.73	18.81					
E51	114.96	176.17	57.24	30.71	38.05		183.14		
R52									
G53	110.26	173.61	44.42						
A54									
P55	139.04		63.4				50.05		
G56	112.17	173.56	44.67						
A57	120.69	177.73	52.64	20.83					
Q58	113.76	178.25	52.95						
L59	125.54	174.09	52.65	38.85	24.25				
I60	105.13	175.14	61.12	38.03	25.37	17.49	13.18		
T61	109.6	172.71	58.19	71.46	22.13				
Y62	123.47	173.01	63.38	36.09					
P63	134.74	178.35	66.55				49.65		
R64	112.12	176.91	59.6	30.91					
A65	119.54	177.6	54.65	19.15					
L66	120.55	179.68	56.73	41.58	26.4				
W67	119.11	175.58	58.69	29.32		110.12	128.32		
W68	118.92	178.9	59.53	28.19		112.58	124.38		
S69	121.71	175.35	62.35	60.63					
V70	123.63	176.78	66.68	30.88	21.85	23.03			

Residue	**N**	**C**	**Cα**	**Cβ**	**C$\gamma2$**	**C$\gamma2$**	**Cδ**	**Cε**	**Cζ**
E71	112.88	175.08	57.64	31.91	31.98			181.74	
T72	118.8	173.96	66.44	67.56	21.7				
A73	124.23	175.96	54.74	18.45					
T74	98.91	175.71	60.61	69.18		21.03			
T75	110.12	171.97	62.6	68.68		21.05			
V76	121.06	178.22	65.74	31.34	22.65	19.76			
G77	100.32	173.75	48.1						
Y78	115.3	177.49	61.04	37.81			130.03	117.55	157.46
G79	101.11	173.82	44.91						
D80	117.85	175.07	54.9	36.75	178.96				
L81	117.33	174.85	52.15	46.35	24.35				
Y82	115.19	171.35	54.9	34.44		128.52		117.63	
P83	131.79	175.6	60.82				48.85		
V84	118.03	175.71	60.14	31.91	20.71	17.63			
T85	116.09	174.05	60.1	72.15		22.14			
L86	122.16	177.47	57.97						
W87	115.14	177.96	58.77	29.05		109.81			
G88	106.74	175.65	45.82						
R89	121.49	177.44	58.72	29.22		27.22	43.68		158.38
L90	119.02	178.97	58.16	40.26	25.68				
V91	117.73	177.55	66.78	30.75	23.11	21.35			
A92	119.48	178.25	55.32	20.03					
V93	117.01	176.84	66.54	31.08	22.95	21.69			
V94	118.34	177.14	66.63	30.86		21.14			
V95	119.08	176.95	66.86	30.77	23.26	21.4			
M96	116.37	176.84	59.35	33.33	32.46				
V97	116.06	178.45	66.33	31.01	23.01	21.63			
A98	124.77	180.33	54.82	18.48					
G99	106.86	174.32	47.17						

Residue	**N**	**C**	**Cα**	**Cβ**	**C$\gamma 2$**	**C$\gamma 2$**	**Cδ**	**Cε**	**Cζ**
I100									
T101									
S102	115.73	174.86	62.94	62.02					
F103	120.2								
G104									
L105									
V106	117.11	176.85	66.37	30.95	23.17	21.42			
T107	116.27	175.63	67.77	67.1		19.64			
A108	121.53	179.55	55.06	17.53					
A109	123.94	177.72	54.85	16.97					
L110	119.23	178.12	57.08	41.95					
A111	117.65	177.21	54.94	16.05					
T112	113.24	176.32	67.02	67.86	19.7				
W113	124.26	178.15	58.14	28.67					
F114									
V115									
G116									
R117									
E118					34.31		181.4		

TABLE S4: Experimental resonance assignments of KcsA in the deactivated state (50 mM KCl, pH 7.5, 9:1 DOPE/DOPS) taken from previous data[1] with re-adjustment of the chemical shift referencing

Residue	**N**	**C**	**Cα**	**Cβ**	**C$\gamma 2$**	**C$\gamma 2$**	**Cδ**	**Cε**	**Cζ**
R27		177.13	59.47	28.84					
A28	119.6	179.78	54.855	17.74					
A29	123.8	179.78	54.78	17.85					
G30	106.75	174.13	47.1						
A31	122.8	178.18	55.025	18.22					
A32									
T33									
V34	120.45	177.63	66.48	30.8					
L35	118.2	177.38	57.82	41.27					
L36	117.85	177.13	57.92	40.57					
V37	117.6	177.33	67.085	30.92					
I38	117.8	176.93	65.725	37.29	28.78	16.78	13.58		
V39	119.75	177.43	66.74	30.81					
L40	118.3	179.28	58.135	41.33					
L41	118.05	179.73	57.305	42.28					
A42	120.15	179.48	53.855	18.58					
G43	109.2	175.18	46.45						
S44	114.7	173.23	63.915	62.83					
Y45	119.5	175.73	61.07	38.35					
L46	116.55	177.18	56.9	41.11					
A47	118.35	177.68	55.095	17.35					
V48	115.85	177.68	64.895	30.88					
L49	115.9	179.48	56.87	41.81					
A50	119.3	178.98	53.92						
E51	114.95	176.43	57.405	30.59	38.38		183.28		
R52	115.75		58.57						
G53	110	173.28	44.205						

Residue	**N**	**C**	**Cα**	**Cβ**	**C$\gamma 2$**	**C$\gamma 2$**	**Cδ**	**Cε**	**Cζ**
A54	123.55		49.665	17.85					
P55	139.3	174.98	63.2	30.97			49.78		
G56	112.3	173.53	44.495						
A57	120.8	177.93	52.8	20.83					
Q58	113.95	178.48	53.135	31.26					
L59	125.3	174.13	52.825	38.99			24.58		
I60	105.25	175.43	61.12	38.19	25.48	17.48	13.38		
T61	109.4	172.88	58.36	71.45		22.28			
Y62	123.5	173.08	63.355	35.97					
P63	134.6	178.38	66.33	30.93			49.63		
R64	111.9	177.03	59.655	31.07					
A65	119.2	177.78	54.69	19.23					
L66	120.45	179.48	57.04	41.43					
W67	118.85	175.38	58.825	29.31	110.48				
W68	118.9	178.93	59.505	28.07	113.08				
S69	121.8	175.48	62.42	60.59					
V70	123.75	176.93	66.75	30.82	23.08	21.58			
E71	112.75	174.98	57.635	31.98	26.58		181.98		
T72	118.75	174.03	66.415	67.58					
A73	124.35	175.73	54.6	18.5					
T74	97.82	175.93	60.715	69.2	21.01				
T75	110.15	172.08	62.62	68.76	21.15				
V76	121.2	178.38	65.66	31.3	22.68	19.78			
G77	100.3	173.88	48.2						
Y78	115.4	177.58	61.045	37.86					
G79	101.33	173.73	45						
D80	117.95	174.93	55.045	36.92	178.98				
L81	117	174.93	52.335	47.22	27.08				
Y82	114.95	171.48	54.8	34.35					

Residue	**N**	**C**	**C**α	**C**β	**C**$\gamma 2$	**C**$\gamma 2$	**C**δ	**C**ε	**C**ζ
P83	131.7	175.88	58.75	31.98			48.79		
V84	117.8	175.73	60.115	32.04	20.78	17.78			
T85	115.95	174.28	60.055	71.95		22.38			
L86	122.15	177.53	57.87	40.79					
W87		178.13	58.595	29.11					
G88	106.85	175.38	45.825						
R89	121.35	177.58	58.89	29.28					
L90	118.25	178.58	58.085	42.36					
V91	117.65	177.28	66.8	30.96					
A92	119.4	178.28	55.37	20.11					
V93	117.25	176.88	66.43						
V94	118.1	177.03	66.7	30.92					
V95	118.5	177.03	66.795	30.85					
M96	116.05	176.68	59.305	33.18	32.48				
V97	115.95	178.48	66.085	31.05					
A98	124.85	179.73	54.93	17.91					
G99	107.05	174.08	47.28						
I100	120.8	177.13	65.5	38.79	25.48	17.78	13.78		
T101	120	176.88	67.1	67.71					
S102	116.6	175.08	62.825	62.07					
F103	120.25	178.68	60.175	37.07					
G104	108	174.53	47.34						
L105	119.4	178.73	58.11	41.13					
V106	117.1	177.08	66.705	30.95					
T107	117.15	175.53	68.19	66.89					
A108	121.05	177.58	54.78	17.3					
A109	118.3	178.08	54.51	17.81					
L110	119.2	177.58	56.76	41.37					
A111									

Residue	**N**	**C**	**Cα**	**Cβ**	**C$\gamma 2$**	**C$\gamma 2$**	**Cδ**	**Cε**	**Cζ**
T112									
W113									
F114									
V115	114.5	178.58	65.98	31.22					
G116	109.8	174.58	47.065						
R117	120.6	174.38	58.34						
E118	116.6		58.66	29.08	35.48		182.28		
Q119									
E120			58.96	27.48	35.68		182.28		

TABLE S5: Chemical shift differences between the activated and deactivated states ($\Delta CS_{exp} = CS_{exp}^{pH=4,act} - CS_{exp}^{pH=7.5,deact}$)

Residue	**N**	**C**	**Cα**	**Cβ**
T33	1.37	-0.29	-0.22	0.03
V34	0.45	-0.46	0.4	0.06
L35				
L36				
V37				
I38	-0.27	0.19	-0.1	-0.15
V39				
L40				
L41				
A42	0.48	-0.18	-0.03	0.02
G43	-0.09	0.06	0.02	
S44	0.09	0.53	-0.04	0.02
Y45	-0.02	0.53	-0.17	0.01
L46				
A47	0.67	-0.05	0.14	0.01

Residue	**N**	**C**	**C$_\alpha$**	**C$_\beta$**
V48	-0.07	-0.02	0.01	-0.21
L49				
A50	-1.68	-0.22	-0.19	
E51	0.01	-0.26	-0.16	0.12
R52				
G53	0.26	0.33	0.22	
A54				
P55	-0.26		0.2	
G56	-0.13	0.03	0.18	
A57	-0.11	-0.2	-0.16	0
Q58	-0.19	-0.23	-0.18	
L59	0.24	-0.04	-0.18	-0.14
I60	-0.12	-0.29	0	-0.16
T61	0.21	-0.17	-0.17	0.01
Y62	-0.02	-0.07	0.02	0.12
P63	0.14	-0.03	0.22	
R64	0.22	-0.12	-0.05	-0.16
A65	0.34	-0.18	-0.04	-0.08
L66	0.1	0.2	-0.31	0.15
W67	0.26	0.19	-0.14	0.01
W68	0.02	-0.03	0.02	0.12
S69	-0.09	-0.13	-0.07	0.04
V70	-0.12	-0.15	-0.07	0.06
E71	0.13	0.09	0	-0.07
T72	0.05	-0.07	0.03	-0.02
A73	-0.12	0.23	0.14	-0.05
T74	1.09	-0.22	-0.1	-0.02
T75	-0.02	-0.11	-0.02	-0.08
V76	-0.14	-0.16	0.08	0.04

Residue	**N**	**C**	**C$_\alpha$**	**C$_\beta$**
G77	0.03	-0.13	-0.1	
Y78	-0.1	-0.09	-0.01	-0.05
G79	-0.22	0.09	-0.09	
D80	-0.1	0.14	-0.14	-0.17
L81	0.33	-0.08	-0.19	-0.87
Y82	0.24	-0.13	0.1	0.09
P83	0.09	-0.28	2.07	
V84	0.23	-0.02	0.03	-0.13
T85	0.14	-0.23	0.05	0.19
L86	0.01	-0.06	0.1	
W87		-0.17	0.17	-0.06
G88	-0.1	0.27	-0.01	
R89	0.15	-0.14	-0.17	-0.06
L90	0.77	0.39	0.08	-2.1
V91	0.08	0.27	-0.02	-0.21
A92	0.08	-0.03	-0.05	-0.08
V93	-0.23	-0.04	0.11	
V94	0.24	0.11	-0.07	-0.06
V95	0.58	-0.08	0.06	-0.09
M96	0.32	0.16	0.04	0.15
V97	0.12	-0.03	0.25	-0.04
A98	-0.08	0.6	-0.11	0.57
G99	-0.19	0.24	-0.11	
I100				
T101				
S102	-0.87	-0.22	0.11	-0.05
F103	-0.05			
G104				
L105				

Residue	N	C	C_α	C_β
V106	0.01	-0.23	-0.33	0
T107	-0.88	0.1	-0.42	0.21
A108	0.48	1.97	0.27	0.23
A109	5.64	-0.37	0.34	-0.84
L110	0.03	0.54	0.32	0.58
A111	0.11	-0.32	0.09	0.2
T112	-0.41	-0.16	0.11	0.27

TABLE S6: Simulated chemical shifts for C_α for the two chemical shift prediction methods and the three channel states. The data represented corresponds to the credible intervals of the chemical shifts that are inferred from the simulation data (CS^{X}_{sim}). The credible intervals are expressed as the center of the interval plus or minus the distance to the upper and lower bounds of the interval. This interval measures our uncertainty of the resonance position in the spectrum and not the peak width which is related to the standard deviation of the skew-normal distribution with which the data is modeled.

Residue	Fully Open, SPARTA+	Partially Open, SPARTA+	Closed, SPARTA+	Fully Open, SHIFTX2	Partially Open, SHIFTX2	Closed, SHIFTX2
I38	65.01 ± 0.03	64.96 ± 0.03	64.84 ± 0.03	64.21 ± 0.02	64.16 ± 0.02	64.09 ± 0.02
A42	55.32 ± 0.01	55.29 ± 0.01	55.27 ± 0.01	55.14 ± 0.02	55.12 ± 0.01	55.13 ± 0.01
G43	47.15 ± 0.01	47.14 ± 0.01	47.12 ± 0.01	47.63 ± 0.01	47.61 ± 0.01	47.56 ± 0.02
S44	62.23 ± 0.02	62.17 ± 0.02	62.51 ± 0.02	62.00 ± 0.02	61.89 ± 0.02	62.09 ± 0.02
Y45	61.72 ± 0.02	61.46 ± 0.02	61.49 ± 0.02	60.95 ± 0.02	60.80 ± 0.02	60.88 ± 0.02
A47	55.14 ± 0.01	55.17 ± 0.01	55.16 ± 0.01	55.14 ± 0.01	55.16 ± 0.01	55.14 ± 0.01
V48	66.06 ± 0.02	66.26 ± 0.02	66.22 ± 0.02	65.91 ± 0.02	66.16 ± 0.02	66.25 ± 0.02
A50	54.27 ± 0.02	54.55 ± 0.01	54.64 ± 0.01	54.47 ± 0.02	54.62 ± 0.01	54.73 ± 0.01
E51	56.39 ± 0.03	56.85 ± 0.04	57.70 ± 0.04	57.19 ± 0.03	57.40 ± 0.04	57.98 ± 0.04
G53	44.90 ± 0.01	44.83 ± 0.01	44.92 ± 0.02	45.52 ± 0.02	45.60 ± 0.02	45.70 ± 0.03
G56	44.57 ± 0.01	44.75 ± 0.01	44.77 ± 0.01	45.19 ± 0.02	45.44 ± 0.02	45.47 ± 0.02
A57	52.32 ± 0.02	52.38 ± 0.02	52.35 ± 0.02	52.26 ± 0.02	52.46 ± 0.02	52.44 ± 0.02
Q58	57.23 ± 0.04	56.59 ± 0.04	56.65 ± 0.03	56.77 ± 0.06	56.16 ± 0.05	56.29 ± 0.05
L59	54.27 ± 0.02	54.53 ± 0.02	54.50 ± 0.02	54.18 ± 0.02	54.32 ± 0.03	54.21 ± 0.02

Residue	Fully Open, SPARTA+	Partially Open, SPARTA+	Closed, SPARTA+	Fully Open, SHIFTX2	Partially Open, SHIFTX2	Closed, SHIFTX2
I60	60.79 ± 0.04	60.77 ± 0.03	60.84 ± 0.03	61.37 ± 0.03	61.01 ± 0.04	61.27 ± 0.03
T61	59.87 ± 0.02	60.72 ± 0.04	60.08 ± 0.02	59.79 ± 0.02	60.71 ± 0.04	59.85 ± 0.02
Y62	63.06 ± 0.03	62.75 ± 0.03	62.54 ± 0.03	61.91 ± 0.02	61.76 ± 0.03	61.67 ± 0.02
R64	59.62 ± 0.01	59.24 ± 0.02	59.41 ± 0.02	59.88 ± 0.02	59.37 ± 0.04	59.72 ± 0.02
A65	55.15 ± 0.01	55.15 ± 0.01	55.18 ± 0.01	55.37 ± 0.01	55.40 ± 0.01	55.45 ± 0.01
L66	58.05 ± 0.01	57.97 ± 0.01	57.92 ± 0.01	57.97 ± 0.01	57.89 ± 0.01	57.91 ± 0.02
W67	60.16 ± 0.02	60.22 ± 0.02	60.29 ± 0.02	60.45 ± 0.02	60.51 ± 0.01	60.49 ± 0.01
W68	60.86 ± 0.02	60.74 ± 0.02	60.57 ± 0.02	60.87 ± 0.02	60.83 ± 0.02	60.80 ± 0.02
S69	62.48 ± 0.01	62.38 ± 0.02	62.22 ± 0.02	62.43 ± 0.01	62.41 ± 0.02	62.20 ± 0.02
V70	66.42 ± 0.02	66.24 ± 0.03	66.35 ± 0.02	66.46 ± 0.02	66.38 ± 0.02	66.48 ± 0.02
E71	58.87 ± 0.02	58.81 ± 0.02	58.69 ± 0.02	59.43 ± 0.03	59.24 ± 0.03	59.04 ± 0.03
T72	65.83 ± 0.01	65.96 ± 0.01	65.98 ± 0.02	66.21 ± 0.02	66.17 ± 0.03	66.20 ± 0.03
A73	54.47 ± 0.01	54.42 ± 0.01	54.40 ± 0.01	54.59 ± 0.02	54.65 ± 0.02	54.62 ± 0.02
T74	63.10 ± 0.04	63.35 ± 0.04	63.47 ± 0.04	62.18 ± 0.04	62.59 ± 0.04	62.58 ± 0.04
T75	63.62 ± 0.01	63.27 ± 0.01	63.38 ± 0.01	63.77 ± 0.02	63.60 ± 0.03	63.58 ± 0.03
V76	64.43 ± 0.03	64.66 ± 0.03	64.70 ± 0.03	64.65 ± 0.02	64.80 ± 0.02	64.84 ± 0.02
G77	45.75 ± 0.01	45.81 ± 0.01	45.80 ± 0.01	46.09 ± 0.01	46.16 ± 0.01	46.20 ± 0.01
Y78	59.48 ± 0.03	60.15 ± 0.02	60.13 ± 0.02	59.98 ± 0.02	60.70 ± 0.01	60.68 ± 0.01
G79	45.33 ± 0.01	45.28 ± 0.00	45.31 ± 0.01	45.55 ± 0.01	45.59 ± 0.01	45.62 ± 0.01
D80	55.47 ± 0.01	55.53 ± 0.01	55.53 ± 0.01	56.24 ± 0.02	56.30 ± 0.02	56.12 ± 0.02
L81	54.05 ± 0.01	54.14 ± 0.02	54.26 ± 0.02	53.76 ± 0.01	53.82 ± 0.02	53.84 ± 0.02
Y82	54.33 ± 0.02	54.34 ± 0.02	54.28 ± 0.02	55.17 ± 0.02	55.21 ± 0.02	55.17 ± 0.02
V84	61.79 ± 0.03	61.65 ± 0.03	61.64 ± 0.02	62.32 ± 0.04	62.18 ± 0.03	62.19 ± 0.03
T85	61.24 ± 0.04	61.37 ± 0.04	61.75 ± 0.04	60.47 ± 0.04	60.59 ± 0.04	60.91 ± 0.04
L86	57.82 ± 0.02	57.97 ± 0.02	58.13 ± 0.01	58.25 ± 0.02	58.21 ± 0.01	58.29 ± 0.01
W87	59.15 ± 0.02	59.07 ± 0.02	59.10 ± 0.03	60.38 ± 0.02	60.17 ± 0.02	60.11 ± 0.03
G88	46.61 ± 0.01	46.65 ± 0.01	46.63 ± 0.01	47.41 ± 0.01	47.43 ± 0.01	47.42 ± 0.01
R89	58.87 ± 0.01	59.08 ± 0.01	59.11 ± 0.01	59.18 ± 0.02	59.51 ± 0.02	59.53 ± 0.02

Residue	Fully Open, SPARTA+	Partially Open, SPARTA+	Closed, SPARTA+	Fully Open, SHIFTX2	Partially Open, SHIFTX2	Closed, SHIFTX2
L90	57.80 ± 0.01	57.87 ± 0.01	57.88 ± 0.01	57.86 ± 0.02	57.93 ± 0.01	57.94 ± 0.02
V91	66.49 ± 0.02	66.49 ± 0.02	66.43 ± 0.02	66.62 ± 0.01	66.56 ± 0.02	66.49 ± 0.02
A92	55.67 ± 0.01	55.62 ± 0.01	55.62 ± 0.01	55.41 ± 0.01	55.39 ± 0.01	55.40 ± 0.01
V93	66.26 ± 0.02	66.75 ± 0.02	66.52 ± 0.03	66.07 ± 0.02	66.23 ± 0.01	66.15 ± 0.02
V94	66.54 ± 0.02	66.59 ± 0.02	66.58 ± 0.02	65.98 ± 0.01	66.01 ± 0.01	66.02 ± 0.01
V95	66.72 ± 0.02	66.74 ± 0.01	66.77 ± 0.02	66.05 ± 0.01	66.11 ± 0.01	66.15 ± 0.01
M96	59.80 ± 0.01	59.10 ± 0.01	59.16 ± 0.01	59.26 ± 0.01	58.92 ± 0.02	59.01 ± 0.02
V97	66.53 ± 0.02	66.31 ± 0.02	66.16 ± 0.02	66.12 ± 0.02	66.12 ± 0.02	66.15 ± 0.02
A98	55.28 ± 0.02	55.05 ± 0.02	55.31 ± 0.01	54.62 ± 0.02	54.72 ± 0.02	54.97 ± 0.01
G99	46.78 ± 0.01	46.93 ± 0.01	46.86 ± 0.01	47.01 ± 0.02	47.31 ± 0.01	47.21 ± 0.01
S102	61.73 ± 0.01	62.17 ± 0.01	62.16 ± 0.01	61.93 ± 0.02	62.29 ± 0.02	62.33 ± 0.02
V106	66.83 ± 0.02	66.88 ± 0.02	67.02 ± 0.02	66.44 ± 0.01	66.45 ± 0.02	66.58 ± 0.02
T107	65.67 ± 0.02	66.94 ± 0.02	67.15 ± 0.01	66.01 ± 0.03	66.86 ± 0.03	67.29 ± 0.01
A108	54.98 ± 0.01	55.14 ± 0.01	55.23 ± 0.01	55.05 ± 0.01	55.14 ± 0.02	55.24 ± 0.01
A109	54.97 ± 0.01	54.98 ± 0.01	54.73 ± 0.01	55.11 ± 0.01	55.22 ± 0.01	55.13 ± 0.01
L110	57.76 ± 0.01	57.69 ± 0.01	57.49 ± 0.01	58.12 ± 0.02	58.10 ± 0.02	57.91 ± 0.01

TABLE S7: Simulated chemical shifts for C_β for the two chemical shift prediction methods and the three channel states. The data represented corresponds to the credible intervals of the chemical shifts that are inferred from the simulation data (CS^{X}_{sim}). The credible intervals are expressed as the center of the interval plus or minus the distance to the upper and lower bounds of the interval. This interval measures our uncertainty of the resonance position in the spectrum and not the peak width which is related to the standard deviation of the skew-normal distribution with which the data is modeled.

Residue	Fully Open, SPARTA+	Partially Open, SPARTA+	Closed, SPARTA+	Fully Open, SHIFTX2	Partially Open, SHIFTX2	Closed, SHIFTX2
I38	37.19 ± 0.02	37.14 ± 0.02	37.07 ± 0.03	37.79 ± 0.01	37.74 ± 0.01	37.69 ± 0.01
A42	18.15 ± 0.00	18.16 ± 0.01	18.15 ± 0.00	18.29 ± 0.01	18.33 ± 0.01	18.29 ± 0.01
S44	63.27 ± 0.01	63.20 ± 0.01	63.30 ± 0.01	62.97 ± 0.01	62.95 ± 0.01	62.94 ± 0.01
Y45	38.75 ± 0.01	38.71 ± 0.01	38.66 ± 0.01	38.32 ± 0.01	38.30 ± 0.01	38.32 ± 0.01

Residue	Fully Open, SPARTA+	Partially Open, SPARTA+	Closed, SPARTA+	Fully Open, SHIFTX2	Partially Open, SHIFTX2	Closed, SHIFTX2
A47	18.18 ± 0.01	18.21 ± 0.01	18.23 ± 0.01	18.39 ± 0.01	18.41 ± 0.01	18.40 ± 0.01
V48	31.33 ± 0.01	31.48 ± 0.01	31.48 ± 0.01	31.45 ± 0.01	31.51 ± 0.01	31.52 ± 0.00
E51	30.09 ± 0.02	30.11 ± 0.02	29.86 ± 0.02	29.90 ± 0.02	29.92 ± 0.02	29.67 ± 0.02
A57	19.68 ± 0.02	19.51 ± 0.02	19.48 ± 0.02	19.38 ± 0.02	19.26 ± 0.02	19.27 ± 0.02
L59	41.63 ± 0.03	41.52 ± 0.04	41.35 ± 0.05	41.86 ± 0.03	41.77 ± 0.04	41.87 ± 0.05
I60	37.70 ± 0.03	38.70 ± 0.06	38.74 ± 0.05	38.13 ± 0.02	38.96 ± 0.05	39.08 ± 0.04
T61	71.49 ± 0.02	70.57 ± 0.05	71.30 ± 0.02	71.28 ± 0.02	70.77 ± 0.04	71.28 ± 0.02
Y62	35.71 ± 0.01	36.21 ± 0.02	35.97 ± 0.01	36.79 ± 0.01	36.78 ± 0.01	36.72 ± 0.01
R64	29.77 ± 0.01	29.59 ± 0.01	29.77 ± 0.01	29.98 ± 0.01	29.72 ± 0.02	29.95 ± 0.01
A65	18.45 ± 0.01	18.43 ± 0.01	18.45 ± 0.01	18.37 ± 0.01	18.38 ± 0.01	18.40 ± 0.01
L66	41.96 ± 0.01	41.92 ± 0.01	41.98 ± 0.01	41.73 ± 0.01	41.73 ± 0.01	41.77 ± 0.01
W67	29.75 ± 0.01	29.57 ± 0.01	29.54 ± 0.01	29.57 ± 0.01	29.46 ± 0.01	29.41 ± 0.01
W68	29.15 ± 0.01	29.24 ± 0.01	29.35 ± 0.01	28.95 ± 0.01	28.99 ± 0.01	28.97 ± 0.01
S69	62.72 ± 0.01	62.72 ± 0.01	62.70 ± 0.01	62.85 ± 0.01	62.94 ± 0.01	62.91 ± 0.01
V70	31.31 ± 0.01	31.41 ± 0.01	31.39 ± 0.01	31.60 ± 0.01	31.66 ± 0.01	31.64 ± 0.01
E71	28.98 ± 0.01	28.82 ± 0.01	28.73 ± 0.01	28.95 ± 0.01	28.95 ± 0.01	28.86 ± 0.01
T72	68.29 ± 0.01	68.28 ± 0.01	68.32 ± 0.01	68.35 ± 0.01	68.39 ± 0.02	68.46 ± 0.02
A73	18.50 ± 0.01	18.64 ± 0.01	18.56 ± 0.01	18.59 ± 0.01	18.59 ± 0.01	18.59 ± 0.01
T74	69.11 ± 0.02	69.27 ± 0.01	69.30 ± 0.01	69.39 ± 0.02	69.37 ± 0.02	69.45 ± 0.01
T75	66.95 ± 0.02	67.02 ± 0.02	67.09 ± 0.02	68.23 ± 0.01	68.15 ± 0.01	68.19 ± 0.01
V76	31.69 ± 0.01	31.61 ± 0.01	31.65 ± 0.01	32.12 ± 0.01	32.09 ± 0.01	32.10 ± 0.01
Y78	38.73 ± 0.01	38.92 ± 0.01	38.92 ± 0.01	38.25 ± 0.01	38.83 ± 0.01	38.86 ± 0.01
D80	40.71 ± 0.01	40.71 ± 0.01	40.70 ± 0.01	40.63 ± 0.01	40.58 ± 0.01	40.41 ± 0.02
L81	44.69 ± 0.02	44.89 ± 0.02	44.80 ± 0.02	44.70 ± 0.03	44.87 ± 0.03	44.90 ± 0.03
Y82	38.52 ± 0.02	38.53 ± 0.02	38.57 ± 0.02	39.98 ± 0.02	40.05 ± 0.02	40.12 ± 0.02
V84	32.97 ± 0.03	33.14 ± 0.03	33.17 ± 0.03	33.47 ± 0.02	33.61 ± 0.02	33.61 ± 0.02
T85	71.12 ± 0.03	71.04 ± 0.03	70.83 ± 0.03	70.87 ± 0.03	70.70 ± 0.03	70.53 ± 0.03
W87	28.75 ± 0.01	28.89 ± 0.01	28.90 ± 0.01	28.78 ± 0.01	28.83 ± 0.01	28.84 ± 0.01

Residue	Fully Open, SPARTA+	Partially Open, SPARTA+	Closed, SPARTA+	Fully Open, SHIFTX2	Partially Open, SHIFTX2	Closed, SHIFTX2
R89	29.47 ± 0.01	29.56 ± 0.01	29.58 ± 0.01	29.44 ± 0.01	29.56 ± 0.01	29.56 ± 0.01
L90	41.74 ± 0.01	41.75 ± 0.01	41.76 ± 0.01	41.63 ± 0.01	41.65 ± 0.01	41.69 ± 0.01
V91	31.27 ± 0.02	31.32 ± 0.01	31.33 ± 0.01	31.55 ± 0.01	31.59 ± 0.01	31.61 ± 0.01
A92	18.63 ± 0.01	18.68 ± 0.00	18.71 ± 0.00	18.56 ± 0.01	18.67 ± 0.01	18.66 ± 0.01
V94	31.27 ± 0.02	31.26 ± 0.01	31.22 ± 0.01	31.75 ± 0.01	31.72 ± 0.00	31.70 ± 0.00
V95	31.38 ± 0.01	31.33 ± 0.01	31.31 ± 0.01	31.49 ± 0.01	31.48 ± 0.01	31.46 ± 0.01
M96	32.42 ± 0.01	32.21 ± 0.01	32.23 ± 0.01	33.01 ± 0.01	32.54 ± 0.01	32.57 ± 0.01
V97	31.39 ± 0.02	31.12 ± 0.02	30.98 ± 0.02	31.76 ± 0.01	31.68 ± 0.01	31.61 ± 0.01
A98	18.37 ± 0.01	18.29 ± 0.01	18.16 ± 0.01	18.71 ± 0.02	18.30 ± 0.01	18.26 ± 0.01
S102	62.86 ± 0.01	62.74 ± 0.01	62.80 ± 0.01	62.86 ± 0.01	62.66 ± 0.01	62.74 ± 0.01
V106	31.33 ± 0.02	31.27 ± 0.02	31.26 ± 0.01	31.56 ± 0.01	31.51 ± 0.01	31.52 ± 0.01
T107	68.13 ± 0.01	68.38 ± 0.01	68.27 ± 0.01	68.47 ± 0.01	68.58 ± 0.01	68.42 ± 0.01
A108	18.08 ± 0.00	18.16 ± 0.00	18.22 ± 0.01	18.21 ± 0.01	18.35 ± 0.01	18.34 ± 0.01
A109	18.31 ± 0.01	18.51 ± 0.01	18.06 ± 0.02	18.30 ± 0.01	18.38 ± 0.01	18.26 ± 0.01
L110	41.62 ± 0.01	41.61 ± 0.01	41.38 ± 0.01	41.54 ± 0.01	41.57 ± 0.01	41.47 ± 0.01

TABLE S8: Simulated chemical shifts for C for the two chemical shift prediction methods and the three channel states. The data represented corresponds to the credible intervals of the chemical shifts that are inferred from the simulation data ($\mathrm{CS}^{\mathrm{X}}_{\mathrm{sim}}$). The credible intervals are expressed as the center of the interval plus or minus the distance to the upper and lower bounds of the interval. This interval measures our uncertainty of the resonance position in the spectrum and not the peak width which is related to the standard deviation of the skew-normal distribution with which the data is modeled.

Residue	Fully Open, SPARTA+	Partially Open, SPARTA+	Closed, SPARTA+	Fully Open, SHIFTX2	Partially Open, SHIFTX2	Closed, SHIFTX2
I38	178.17 ± 0.01	178.12 ± 0.01	178.16 ± 0.01	178.48 ± 0.01	178.44 ± 0.01	178.48 ± 0.01
A42	179.86 ± 0.00	179.83 ± 0.00	179.84 ± 0.00	180.15 ± 0.01	180.15 ± 0.01	180.15 ± 0.01
G43	176.50 ± 0.01	176.53 ± 0.01	176.49 ± 0.01	175.99 ± 0.02	175.99 ± 0.02	176.18 ± 0.02
S44	176.21 ± 0.01	176.27 ± 0.01	176.23 ± 0.01	176.22 ± 0.01	176.26 ± 0.01	176.17 ± 0.01
Y45	177.51 ± 0.01	177.45 ± 0.01	177.29 ± 0.01	178.24 ± 0.02	178.10 ± 0.02	178.09 ± 0.02

Residue	Fully Open, SPARTA+	Partially Open, SPARTA+	Closed, SPARTA+	Fully Open, SHIFTX2	Partially Open, SHIFTX2	Closed, SHIFTX2
A47	179.33 ± 0.01	179.30 ± 0.01	179.31 ± 0.01	178.89 ± 0.01	178.86 ± 0.01	178.91 ± 0.01
V48	178.17 ± 0.01	178.13 ± 0.01	178.15 ± 0.01	177.78 ± 0.02	177.91 ± 0.02	177.81 ± 0.02
A50	179.07 ± 0.02	179.45 ± 0.02	179.70 ± 0.02	178.67 ± 0.03	179.26 ± 0.02	179.61 ± 0.02
E51	176.61 ± 0.03	177.35 ± 0.04	178.11 ± 0.05	176.28 ± 0.02	176.70 ± 0.04	177.36 ± 0.04
G53	173.82 ± 0.02	173.91 ± 0.02	173.99 ± 0.02	173.92 ± 0.01	174.03 ± 0.02	174.13 ± 0.02
G56	173.87 ± 0.02	174.15 ± 0.02	174.16 ± 0.01	174.36 ± 0.01	174.44 ± 0.01	174.43 ± 0.01
A57	177.53 ± 0.03	177.30 ± 0.02	177.39 ± 0.03	177.56 ± 0.02	177.57 ± 0.02	177.48 ± 0.01
Q58	176.56 ± 0.02	176.18 ± 0.03	176.03 ± 0.03	176.20 ± 0.02	175.86 ± 0.03	175.89 ± 0.02
L59	176.75 ± 0.03	176.14 ± 0.04	175.91 ± 0.03	176.47 ± 0.01	176.16 ± 0.03	176.29 ± 0.02
I60	174.91 ± 0.02	174.95 ± 0.02	174.85 ± 0.02	175.14 ± 0.01	175.03 ± 0.03	175.01 ± 0.03
T61	174.87 ± 0.02	174.81 ± 0.02	175.00 ± 0.02	174.95 ± 0.02	175.04 ± 0.01	174.96 ± 0.02
Y62	176.18 ± 0.01	175.98 ± 0.02	176.04 ± 0.01	176.39 ± 0.05	176.10 ± 0.05	176.24 ± 0.04
P63	178.99 ± 0.01	178.93 ± 0.01	178.83 ± 0.01	179.35 ± 0.02	179.41 ± 0.02	179.30 ± 0.02
R64	178.58 ± 0.01	178.59 ± 0.01	178.49 ± 0.01	178.49 ± 0.01	178.54 ± 0.01	178.48 ± 0.01
A65	179.83 ± 0.01	179.89 ± 0.01	179.85 ± 0.01	179.65 ± 0.01	179.61 ± 0.01	179.48 ± 0.01
L66	178.15 ± 0.01	178.18 ± 0.01	178.35 ± 0.02	178.88 ± 0.01	178.88 ± 0.01	178.96 ± 0.02
W67	177.75 ± 0.01	177.72 ± 0.01	177.67 ± 0.01	177.37 ± 0.01	177.42 ± 0.02	177.41 ± 0.02
W68	178.03 ± 0.01	178.15 ± 0.01	178.27 ± 0.01	177.21 ± 0.02	177.20 ± 0.02	177.20 ± 0.02
S69	176.29 ± 0.01	176.32 ± 0.01	176.37 ± 0.01	175.65 ± 0.02	175.72 ± 0.02	175.73 ± 0.02
V70	177.38 ± 0.02	177.24 ± 0.02	177.37 ± 0.02	177.36 ± 0.02	177.55 ± 0.02	177.54 ± 0.02
E71	178.99 ± 0.01	178.80 ± 0.01	178.78 ± 0.01	178.23 ± 0.02	178.04 ± 0.02	178.03 ± 0.02
T72	176.24 ± 0.01	176.37 ± 0.01	176.38 ± 0.01	175.58 ± 0.02	175.56 ± 0.02	175.58 ± 0.02
A73	178.56 ± 0.02	178.72 ± 0.03	179.16 ± 0.02	178.56 ± 0.02	178.80 ± 0.02	178.71 ± 0.02
T74	174.95 ± 0.02	175.00 ± 0.02	174.94 ± 0.02	174.68 ± 0.01	174.57 ± 0.01	174.73 ± 0.01
T75	174.68 ± 0.02	174.76 ± 0.02	174.77 ± 0.02	173.63 ± 0.01	173.54 ± 0.01	173.57 ± 0.01
V76	176.92 ± 0.01	176.99 ± 0.01	177.06 ± 0.01	175.51 ± 0.01	175.56 ± 0.01	175.59 ± 0.01
G77	175.82 ± 0.02	175.83 ± 0.01	175.84 ± 0.01	174.47 ± 0.01	174.52 ± 0.01	174.55 ± 0.01
Y78	176.84 ± 0.01	176.83 ± 0.01	176.98 ± 0.01	176.40 ± 0.01	176.46 ± 0.01	176.46 ± 0.01

Residue	**Fully Open, SPARTA+**	**Partially Open, SPARTA+**	**Closed, SPARTA+**	**Fully Open, SHIFTX2**	**Partially Open, SHIFTX2**	**Closed, SHIFTX2**
G79	174.87 ± 0.01	174.98 ± 0.01	174.99 ± 0.01	173.50 ± 0.01	173.56 ± 0.02	173.65 ± 0.02
D80	176.12 ± 0.01	176.10 ± 0.01	176.09 ± 0.02	175.31 ± 0.01	175.33 ± 0.01	175.30 ± 0.01
L81	174.60 ± 0.02	174.52 ± 0.02	174.47 ± 0.02	174.99 ± 0.02	175.05 ± 0.02	174.99 ± 0.02
Y82	172.89 ± 0.01	172.87 ± 0.01	172.87 ± 0.01	172.38 ± 0.01	172.37 ± 0.01	172.39 ± 0.01
P83	176.00 ± 0.02	175.91 ± 0.02	175.82 ± 0.02	176.03 ± 0.01	176.03 ± 0.01	175.99 ± 0.01
V84	175.80 ± 0.02	175.68 ± 0.02	175.74 ± 0.02	176.03 ± 0.02	176.08 ± 0.02	176.09 ± 0.02
T85	175.33 ± 0.02	175.47 ± 0.01	175.50 ± 0.01	174.85 ± 0.01	174.91 ± 0.01	174.91 ± 0.01
L86	177.59 ± 0.01	177.78 ± 0.02	177.78 ± 0.01	178.52 ± 0.01	178.63 ± 0.02	178.63 ± 0.02
W87	178.51 ± 0.01	178.47 ± 0.01	178.46 ± 0.01	178.82 ± 0.01	178.72 ± 0.02	178.74 ± 0.02
G88	176.01 ± 0.01	176.05 ± 0.01	176.07 ± 0.01	175.83 ± 0.02	175.76 ± 0.02	175.82 ± 0.02
R89	178.48 ± 0.01	178.49 ± 0.01	178.50 ± 0.01	178.21 ± 0.02	178.23 ± 0.02	178.25 ± 0.02
L90	178.91 ± 0.01	178.88 ± 0.01	178.91 ± 0.01	179.82 ± 0.01	179.79 ± 0.01	179.76 ± 0.01
V91	177.84 ± 0.01	177.89 ± 0.01	177.87 ± 0.01	177.71 ± 0.01	177.78 ± 0.01	177.78 ± 0.01
A92	179.74 ± 0.01	179.76 ± 0.01	179.76 ± 0.01	179.20 ± 0.01	179.14 ± 0.01	179.18 ± 0.01
V93	177.93 ± 0.01	177.99 ± 0.01	177.94 ± 0.01	178.01 ± 0.01	178.03 ± 0.01	177.95 ± 0.02
V94	178.17 ± 0.01	178.13 ± 0.01	178.15 ± 0.01	178.22 ± 0.01	178.30 ± 0.01	178.34 ± 0.01
V95	178.19 ± 0.01	178.12 ± 0.01	178.06 ± 0.01	178.06 ± 0.01	178.03 ± 0.01	177.83 ± 0.01
M96	178.92 ± 0.01	178.46 ± 0.01	178.48 ± 0.01	178.38 ± 0.02	177.86 ± 0.02	177.87 ± 0.01
V97	177.77 ± 0.02	178.00 ± 0.01	177.99 ± 0.01	178.13 ± 0.01	178.01 ± 0.02	178.00 ± 0.02
A98	179.77 ± 0.01	179.62 ± 0.01	179.55 ± 0.01	180.00 ± 0.02	179.98 ± 0.02	180.06 ± 0.02
G99	176.08 ± 0.01	175.77 ± 0.01	175.82 ± 0.02	175.66 ± 0.03	175.03 ± 0.02	175.15 ± 0.03
S102	176.38 ± 0.01	176.31 ± 0.01	176.28 ± 0.01	176.02 ± 0.01	175.87 ± 0.01	175.94 ± 0.01
V106	178.06 ± 0.01	178.06 ± 0.01	178.01 ± 0.01	177.87 ± 0.02	177.95 ± 0.02	177.99 ± 0.02
T107	176.18 ± 0.01	176.36 ± 0.01	176.26 ± 0.01	176.06 ± 0.02	176.04 ± 0.01	175.96 ± 0.01
A108	179.13 ± 0.01	179.15 ± 0.01	179.22 ± 0.01	179.62 ± 0.02	179.23 ± 0.01	179.34 ± 0.02
A109	179.71 ± 0.01	179.52 ± 0.01	179.15 ± 0.02	179.58 ± 0.02	179.36 ± 0.01	179.40 ± 0.02
L110	179.15 ± 0.01	178.96 ± 0.01	178.67 ± 0.01	179.44 ± 0.02	179.22 ± 0.02	178.77 ± 0.02

TABLE S9: Simulated chemical shifts for N for the two chemical shift prediction methods and the three channel states. The data represented corresponds to the credible intervals of the chemical shifts that are inferred from the simulation data (CS^{X}_{sim}). The credible intervals are expressed as the center of the interval plus or minus the distance to the upper and lower bounds of the interval. This interval measures our uncertainty of the resonance position in the spectrum and not the peak width which is related to the standard deviation of the skew-normal distribution with which the data is modeled.

Residue	Fully Open, SPARTA+	Partially Open, SPARTA+	Closed, SPARTA+	Fully Open, SHIFTX2	Partially Open, SHIFTX2	Closed, SHIFTX2
I38	120.04 ± 0.02	119.88 ± 0.03	119.88 ± 0.03	119.50 ± 0.04	119.38 ± 0.05	119.48 ± 0.04
A42	121.09 ± 0.02	121.15 ± 0.03	121.10 ± 0.02	121.41 ± 0.05	121.49 ± 0.05	121.52 ± 0.05
G43	106.46 ± 0.03	106.47 ± 0.03	106.32 ± 0.03	105.87 ± 0.05	105.82 ± 0.06	105.84 ± 0.06
S44	119.13 ± 0.02	119.13 ± 0.02	118.93 ± 0.02	116.45 ± 0.04	116.29 ± 0.04	116.64 ± 0.04
Y45	123.91 ± 0.04	123.97 ± 0.04	123.31 ± 0.03	121.70 ± 0.04	121.69 ± 0.04	121.38 ± 0.04
A47	122.15 ± 0.03	122.30 ± 0.03	122.29 ± 0.03	121.14 ± 0.05	121.28 ± 0.05	121.32 ± 0.05
V48	119.05 ± 0.03	119.07 ± 0.03	119.49 ± 0.02	117.27 ± 0.05	117.30 ± 0.05	117.55 ± 0.04
A50	120.53 ± 0.04	120.74 ± 0.03	120.56 ± 0.03	119.94 ± 0.05	120.21 ± 0.05	120.44 ± 0.05
E51	116.49 ± 0.06	116.49 ± 0.04	117.13 ± 0.04	115.80 ± 0.09	115.50 ± 0.07	116.40 ± 0.09
G53	109.13 ± 0.08	109.00 ± 0.07	108.18 ± 0.07	110.11 ± 0.13	109.94 ± 0.14	108.72 ± 0.14
G56	110.07 ± 0.08	110.28 ± 0.08	110.50 ± 0.07	109.65 ± 0.12	110.13 ± 0.11	110.48 ± 0.09
A57	122.54 ± 0.05	122.16 ± 0.05	122.11 ± 0.04	122.66 ± 0.07	122.90 ± 0.05	122.89 ± 0.05
Q58	119.73 ± 0.06	120.33 ± 0.07	120.43 ± 0.06	119.11 ± 0.09	119.74 ± 0.09	120.12 ± 0.09
L59	118.56 ± 0.09	120.09 ± 0.08	120.40 ± 0.07	117.30 ± 0.10	119.18 ± 0.12	119.59 ± 0.09
I60	114.79 ± 0.11	117.17 ± 0.20	117.76 ± 0.18	115.24 ± 0.14	117.91 ± 0.25	119.20 ± 0.26
T61	111.83 ± 0.07	113.05 ± 0.09	111.85 ± 0.06	112.03 ± 0.11	113.62 ± 0.17	111.73 ± 0.10
Y62	124.60 ± 0.08	125.25 ± 0.09	123.96 ± 0.07	123.68 ± 0.08	124.70 ± 0.09	124.00 ± 0.09
R64	118.64 ± 0.03	118.42 ± 0.03	118.70 ± 0.03	118.87 ± 0.05	118.74 ± 0.06	119.08 ± 0.06
A65	122.76 ± 0.02	122.85 ± 0.02	122.81 ± 0.02	121.75 ± 0.05	121.82 ± 0.05	121.78 ± 0.05
L66	120.96 ± 0.02	120.90 ± 0.03	120.85 ± 0.03	120.04 ± 0.04	120.04 ± 0.05	120.07 ± 0.05
W67	120.87 ± 0.02	120.66 ± 0.03	120.78 ± 0.03	120.62 ± 0.04	120.62 ± 0.04	120.67 ± 0.04
W68	121.41 ± 0.02	121.56 ± 0.02	121.85 ± 0.03	119.78 ± 0.05	119.62 ± 0.04	119.56 ± 0.04
S69	115.53 ± 0.02	115.51 ± 0.02	115.53 ± 0.02	115.34 ± 0.04	115.42 ± 0.04	115.10 ± 0.05
V70	121.42 ± 0.03	121.44 ± 0.04	121.87 ± 0.05	120.28 ± 0.05	120.00 ± 0.07	120.55 ± 0.06
E71	119.07 ± 0.04	118.95 ± 0.05	118.77 ± 0.04	118.47 ± 0.07	118.47 ± 0.09	118.29 ± 0.09

Residue	Fully Open, SPARTA+	Partially Open, SPARTA+	Closed, SPARTA+	Fully Open, SHIFTX2	Partially Open, SHIFTX2	Closed, SHIFTX2
T72	115.95 ± 0.04	116.39 ± 0.04	116.71 ± 0.04	115.35 ± 0.08	115.83 ± 0.08	115.95 ± 0.07
A73	122.82 ± 0.03	122.89 ± 0.03	122.82 ± 0.03	122.91 ± 0.08	123.09 ± 0.07	122.92 ± 0.07
T74	108.09 ± 0.05	108.18 ± 0.05	108.79 ± 0.05	106.89 ± 0.09	107.41 ± 0.11	107.34 ± 0.10
T75	110.40 ± 0.04	110.36 ± 0.04	110.28 ± 0.04	114.93 ± 0.03	114.72 ± 0.03	114.83 ± 0.03
V76	120.81 ± 0.05	121.13 ± 0.04	121.16 ± 0.05	120.66 ± 0.04	120.73 ± 0.03	120.79 ± 0.03
G77	106.44 ± 0.03	106.42 ± 0.02	106.42 ± 0.02	108.85 ± 0.04	108.83 ± 0.04	108.73 ± 0.03
Y78	121.98 ± 0.06	121.96 ± 0.06	121.99 ± 0.06	119.92 ± 0.10	120.53 ± 0.10	120.39 ± 0.11
G79	102.76 ± 0.04	102.63 ± 0.03	102.77 ± 0.03	106.09 ± 0.03	106.15 ± 0.03	106.27 ± 0.03
D80	119.19 ± 0.03	119.19 ± 0.03	119.09 ± 0.03	119.27 ± 0.04	119.43 ± 0.04	119.41 ± 0.04
L81	118.27 ± 0.10	118.35 ± 0.08	118.52 ± 0.07	117.99 ± 0.07	118.07 ± 0.07	118.09 ± 0.06
Y82	116.64 ± 0.08	116.96 ± 0.08	117.23 ± 0.08	118.12 ± 0.10	118.08 ± 0.10	118.35 ± 0.10
V84	117.15 ± 0.15	117.43 ± 0.12	117.69 ± 0.12	119.33 ± 0.13	119.08 ± 0.11	119.16 ± 0.11
T85	113.79 ± 0.06	113.74 ± 0.05	114.20 ± 0.05	111.26 ± 0.12	111.18 ± 0.11	111.73 ± 0.10
L86	123.75 ± 0.07	123.65 ± 0.05	124.07 ± 0.05	124.13 ± 0.07	123.95 ± 0.07	124.37 ± 0.06
W87	117.81 ± 0.03	117.71 ± 0.03	117.57 ± 0.03	117.41 ± 0.05	117.33 ± 0.06	117.30 ± 0.05
G88	106.96 ± 0.03	107.25 ± 0.03	107.32 ± 0.04	106.76 ± 0.07	106.98 ± 0.06	107.07 ± 0.06
R89	122.13 ± 0.02	122.21 ± 0.02	122.20 ± 0.02	120.42 ± 0.04	120.72 ± 0.03	120.73 ± 0.03
L90	120.25 ± 0.03	120.37 ± 0.03	120.34 ± 0.03	119.40 ± 0.05	119.46 ± 0.05	119.41 ± 0.05
V91	119.11 ± 0.02	118.93 ± 0.03	118.95 ± 0.03	119.03 ± 0.04	118.83 ± 0.05	118.61 ± 0.07
A92	122.81 ± 0.03	122.79 ± 0.02	122.73 ± 0.03	121.10 ± 0.05	121.05 ± 0.05	121.08 ± 0.06
V93	118.22 ± 0.05	118.84 ± 0.03	117.95 ± 0.06	117.34 ± 0.05	117.66 ± 0.04	117.36 ± 0.06
V94	119.72 ± 0.04	119.46 ± 0.02	119.77 ± 0.03	119.23 ± 0.07	119.34 ± 0.05	119.41 ± 0.04
V95	120.11 ± 0.03	119.85 ± 0.02	119.81 ± 0.02	119.48 ± 0.05	119.58 ± 0.04	119.55 ± 0.04
M96	119.27 ± 0.02	118.11 ± 0.04	118.22 ± 0.04	118.11 ± 0.03	117.42 ± 0.06	117.53 ± 0.05
V97	119.45 ± 0.02	120.45 ± 0.04	120.11 ± 0.05	118.14 ± 0.05	119.21 ± 0.06	119.06 ± 0.07
A98	121.15 ± 0.03	121.98 ± 0.03	122.40 ± 0.03	121.01 ± 0.06	121.44 ± 0.05	121.79 ± 0.05
G99	107.39 ± 0.03	107.91 ± 0.02	107.51 ± 0.02	104.73 ± 0.08	105.54 ± 0.05	105.28 ± 0.04
S102	118.34 ± 0.02	118.80 ± 0.02	118.54 ± 0.03	115.28 ± 0.07	116.46 ± 0.05	116.55 ± 0.04

Residue	Fully Open, SPARTA+	Partially Open, SPARTA+	Closed, SPARTA+	Fully Open, SHIFTX2	Partially Open, SHIFTX2	Closed, SHIFTX2
F103	123.52 ± 0.03	121.27 ± 0.04	122.08 ± 0.07	121.95 ± 0.05	120.11 ± 0.07	120.72 ± 0.08
V106	118.68 ± 0.04	118.22 ± 0.06	118.87 ± 0.03	118.51 ± 0.06	117.92 ± 0.09	118.61 ± 0.05
T107	113.80 ± 0.05	115.97 ± 0.06	116.68 ± 0.02	112.95 ± 0.11	115.22 ± 0.12	116.47 ± 0.05
A108	123.63 ± 0.02	123.83 ± 0.03	123.81 ± 0.02	123.47 ± 0.06	122.67 ± 0.07	122.26 ± 0.05
A109	121.81 ± 0.02	121.99 ± 0.02	121.73 ± 0.02	120.50 ± 0.04	120.58 ± 0.04	120.79 ± 0.04
L110	119.47 ± 0.02	119.89 ± 0.02	119.48 ± 0.02	118.66 ± 0.04	118.94 ± 0.04	118.86 ± 0.04

TABLE S10: Difference between simulated and experimental chemical shifts for C_α for the two chemical shift prediction methods and the Fully Open and Fully Partially states ($CS^{FO}_{sim} - CS^{PO}_{sim}$). The first 4 columns show the relative chemical shifts using the closed state as a reference.

Residue	Fully Open, SPARTA+	Partially Open, SPARTA+	Fully Open, SHIFTX2	Partially Open, SHIFTX2	Fully Open, SPARTA+	Partially Open, SPARTA+	Fully Open, SHIFTX2	Partially Open, SHIFTX2
A50	0.5±0.0	0.8±0.0			-0.17±0.02	0.11±0.02		
G56			0.5±0.0	0.8±0.0			-0.45±0.02	-0.21±0.02
Q58	4.3±0.0	3.6±0.0			0.77±0.05	0.12±0.05		
T61	1.7±0.0	2.5±0.0	1.6±0.0	2.5±0.0	-0.04±0.03	0.81±0.05	0.11±0.03	1.03±0.05
R64	0.0±0.0	-0.4±0.0	0.3±0.0	-0.2±0.0	0.26±0.02	-0.12±0.03	0.21±0.03	-0.29±0.04
T75	1.0±0.0	0.7±0.0			0.26±0.02	-0.08±0.02		
Y78	-1.6±0.0	-0.9±0.0	-1.1±0.0	-0.3±0.0	-0.65±0.04	0.03±0.03	-0.69±0.03	0.03±0.02
R89	0.1±0.0	0.4±0.0	0.5±0.0	0.8±0.0	-0.07±0.02	0.15±0.02	-0.18±0.03	0.15±0.02
V93	-0.3±0.0	0.2±0.0			-0.37±0.04	0.12±0.04		
M96	0.4±0.0	-0.2±0.0	-0.1±0.0	-0.4±0.0	0.59±0.02	-0.11±0.02	0.20±0.02	-0.14±0.02
A98	0.5±0.0	0.2±0.0			0.08±0.02	-0.15±0.02		
G99			-0.2±0.0	0.1±0.0			-0.08±0.02	0.21±0.02
S102	-1.2±0.0	-0.8±0.0	-1.0±0.0	-0.7±0.0	-0.55±0.02	-0.11±0.02	-0.52±0.03	-0.16±0.02
T107	-2.1±0.0	-0.8±0.0	-1.8±0.0	-0.9±0.0	-1.06±0.02	0.21±0.02	-0.86±0.04	-0.02±0.03

TABLE S11: Difference between simulated and experimental chemical shifts for C_β for the two chemical shift prediction methods and the Partially Open and Fully Open states ($CS^{FO}_{sim} - CS^{PO}_{sim}$). The first 4 columns show the relative chemical shifts using the closed state as a reference.

Residue	**Fully Open, SPARTA+**	**Partially Open, SPARTA+**	**Fully Open, SHIFTX2**	**Partially Open, SHIFTX2**	**Fully Open, SPARTA+**	**Partially Open, SPARTA+**	**Fully Open, SHIFTX2**	**Partially Open, SHIFTX2**
I60	-0.3±0.0	0.7±0.1	0.1±0.0	0.9±0.0	-0.88±0.06	0.12±0.08	-0.79±0.04	0.05±0.06
T61	0.0±0.0	-0.9±0.0	-0.2±0.0	-0.7±0.0	0.17±0.03	-0.74±0.05	-0.01±0.03	-0.52±0.04
Y62	-0.4±0.0	0.1±0.0			-0.38±0.02	0.12±0.02		
R64			-0.9±0.0	-1.2±0.0			0.19±0.01	-0.07±0.02
Y78			0.4±0.0	1.0±0.0			-0.57±0.02	0.01±0.01
M96	-0.9±0.0	-1.1±0.0	-0.3±0.0	-0.8±0.0	0.04±0.01	-0.17±0.01	0.28±0.02	-0.18±0.02
V97	0.4±0.0	0.1±0.0			0.45±0.02	0.17±0.02		
A98			0.2±0.0	-0.2±0.0			-0.11±0.02	-0.52±0.01
S102			0.8±0.0	0.6±0.0			0.17±0.02	-0.04±0.02
T107	1.0±0.0	1.3±0.0			-0.35±0.01	-0.10±0.01		
A109	1.3±0.0	1.5±0.0			1.09±0.02	1.29±0.02		

TABLE S12: Difference between simulated and experimental chemical shifts for C for the two chemical shift prediction methods and the Partially Open and Fully Open states ($CS^{FO}_{sim} - CS^{PO}_{sim}$). The first 4 columns show the relative chemical shifts using the closed state as a reference.

Residue	**Fully Open, SPARTA+**	**Partially Open, SPARTA+**	**Fully Open, SHIFTX2**	**Partially Open, SHIFTX2**	**Fully Open, SPARTA+**	**Partially Open, SPARTA+**	**Fully Open, SHIFTX2**	**Partially Open, SHIFTX2**
A50	0.3±0.0	0.7±0.0	-0.1±0.0	0.5±0.0	-0.41±0.03	-0.03±0.03	-0.73±0.04	-0.13±0.03
E51	0.4±0.0	1.2±0.0			-1.25±0.05	-0.50±0.06		
G56	0.3±0.0	0.6±0.0			-0.32±0.03	-0.04±0.02		
Q58	-1.7±0.0	-2.1±0.0			0.76±0.04	0.38±0.04		
L59	2.7±0.0	2.1±0.0			0.88±0.04	0.27±0.05		
M96	2.1±0.0	1.6±0.0	1.5±0.0	1.0±0.0	0.28±0.01	-0.18±0.02	0.35±0.02	-0.17±0.02
V97	-0.7±0.0	-0.4±0.0			-0.18±0.02	0.05±0.02		
G99	1.8±0.0	1.4±0.0	1.3±0.0	0.7±0.0	0.02±0.02	-0.29±0.02	0.27±0.04	-0.35±0.03

Residue	Fully Open, SPARTA+	Partially Open, SPARTA+	Fully Open, SHIFTX2	Partially Open, SHIFTX2	Fully Open, SPARTA+	Partially Open, SPARTA+	Fully Open, SHIFTX2	Partially Open, SHIFTX2
A108			0.1±0.0	-0.3±0.0			-1.70±0.03	-2.08±0.02
A109			1.9±0.0	1.6±0.0			0.54±0.02	0.32±0.02

TABLE S13: Difference between simulated and experimental chemical shifts for N for the two chemical shift prediction methods and the Partially Open and Fully Open states ($CS^{FO}_{sim} - CS^{PO}_{sim}$). The first 4 columns show the relative chemical shifts using the closed state as a reference.

Residue	Fully Open, SPARTA+	Partially Open, SPARTA+	Fully Open, SHIFTX2	Partially Open, SHIFTX2	Fully Open, SPARTA+	Partially Open, SPARTA+	Fully Open, SHIFTX2	Partially Open, SHIFTX2
L59	-7.0±0.1	-5.4±0.1	-8.2±0.1	-6.4±0.1	-2.07±0.11	-0.54±0.11	-2.53±0.14	-0.65±0.15
I60			10.1±0.1	12.8±0.3			-3.81±0.30	-1.17±0.37
T61			2.4±0.1	4.0±0.2			0.09±0.15	1.68±0.20
Y62			0.2±0.1	1.2±0.1			-0.29±0.12	0.74±0.12
V93	1.2±0.0	1.8±0.0			0.51±0.08	1.12±0.06		
M96	2.9±0.0	1.7±0.0	1.7±0.0	1.0±0.1	0.73±0.04	-0.42±0.05	0.26±0.06	-0.44±0.08
V97	3.4±0.0	4.4±0.0	2.1±0.1	3.2±0.1	-0.76±0.05	0.23±0.06	-1.03±0.09	0.04±0.10
A98	-3.6±0.0	-2.8±0.0			-1.18±0.04	-0.34±0.04		
G99	0.5±0.0	1.1±0.0	-2.1±0.1	-1.3±0.1	0.06±0.04	0.59±0.03	-0.38±0.09	0.44±0.07
S102			-0.5±0.1	0.7±0.0			-0.40±0.08	0.79±0.06
F103	3.3±0.0	1.1±0.0	1.7±0.1	-0.1±0.1	1.50±0.08	-0.76±0.08	1.27±0.09	-0.57±0.10
T107	-2.5±0.0	-0.3±0.1	-3.3±0.1	-1.1±0.1	-2.01±0.05	0.17±0.07	-2.63±0.12	-0.38±0.13
A108			1.9±0.1	1.1±0.1			0.72±0.08	-0.08±0.09

REFERENCES

[1]B. J. Wylie, M. P. Bhate, and A. E. McDermott, “Transmembrane allosteric coupling of the gates in a potassium channel,” Proceedings of the National Academy of Sciences of the United States of America **111**, 185–190 (2014).